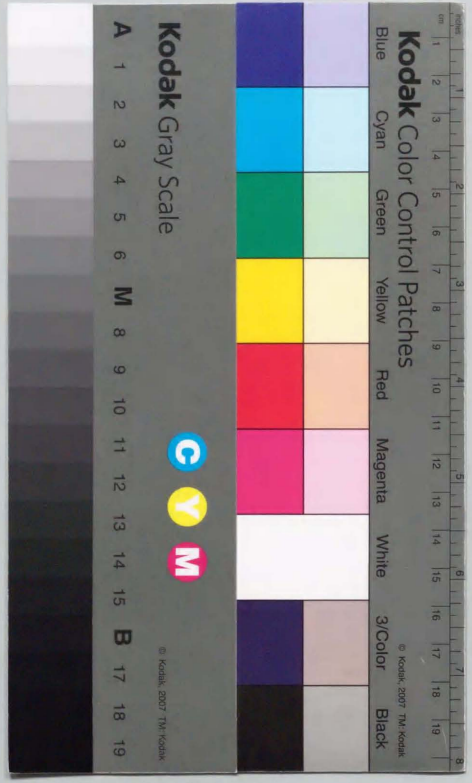

学位論文

Mechanisms of the Seasonal Variation of Chlorophyll in the North Pacific: A Study Using an Ecosystem Model Embedded in an Ocean General Circulation Model.

(北太平洋におけるクロロフィルの季節変動のメカニズム： 海洋大循環モデルに組み入れた生態系モデルを用いた研究.)

平成９年６月博士(理学)申請

東京大学大学院理学系研究科
地球惑星物理学専攻
河宮 未知生

Abstract

The role of physical environments in forming the seasonal variation of chlorophyll in the North Pacific is investigated. An ecosystem model is developed and embedded in an ocean general circulation model (OGCM).

The ecosystem model is first calibrated by applying its vertical one-dimensional version to the Ocean Weather Station (OWS) Papa and the Bermuda Atlantic Time-series Study (BATS) site. The two sites have extremely different oceanographic characteristics to each other because the former is located in a eutrophic, subpolar region while the latter is in an oligotrophic, subtropical region. With only a few parameters changed, the model can reproduce the contrast between the sites that nitrate is far more abundant at OWS Papa than at the BATS site, while chlorophyll abundance and primary production are only moderately higher at the former. The parameter changes are justifiable on the basis of observation.

The ecosystem model is then incorporated into an OGCM and the combined model is applied to the North Pacific. The OGCM shows a good skill in providing realistic physical environments concerning the mixed layer depth (MLD) and the vertical flow except for the MLD off Sanriku and on both sides of the equator. The model results for nitrate, chlorophyll, zooplankton, and net primary production are well compared to the observations. However, discrepancies between the model results and the observations are found. Some of them may be ascribed to the photoadaptation process which is not included in the model or the simple extrapolation of the temperature dependence of photosynthesis. In spite of these defects, the model results are acceptable because the orders of the values are within those of the observations and the overall pattern is that the values are low in the subtropical region and high in the subpolar and the equatorial region, as the observations show.

According to the seasonal variation pattern of chlorophyll in the model, the North Pacific can be divided into seven areas. It is shown that the physical factors determining the modeled seasonal variations are the vertical flow, the vertical mixing, and less importantly, the solar radiation. Various combinations of these factors result in diverse patterns, but it is possible to classify them comprehensively in terms of the amplitude of the seasonal variation of MLD

and the annual mean vertical flow. The areal division and the seasonal variation of each area are similar to the observations, suggesting that the differences in physical environments are able to yield most of the diversity of the observed seasonal patterns.

The results of the model are encouraging also for its future application to the decadal variation of the ecosystem, since it is demonstrated that the model is able to reproduce the regional differences in response of the ecosystem to changes in MLD.

Acknowledgments

I would like to express my heartfelt gratitude to Prof. Nobuo Suginohara and Dr. Michio J. Kishi for the stimulating discussions, their continuous encouragements, and their critical reading of the manuscript. I would also like to appreciate the helpful comments of Dr. Yasuhiro Yamanaka. Thanks are also extended to Mr. Ryo Furue, Dr. Hiroyasu Hasumi, Mr. Hiroyuki Tsujino, Mr. Hideyuki Nakano, Ms. Midori Miki, Mr. Hideki Mizukami, and Mr. Tomohiko Tsunoda in the Ocean Modeling Group of the Center for Climate System Research. My gratitude should be devoted to Prof. Takashige Sugimoto, Dr. Hideaki Nakata, Dr. Shingo Kimura, Dr. Kazuaki Tadokoro, Dr. M. D. Kawser Ahmed, Ms. Susana Sainz-Trapaga, Ms. Yuko Oshima, and other members in the Division of Fisheries Environmental Oceanography of Ocean Research Institute for receiving me as a participant to their seminar, where I learned a lot on biological oceanography. Discussions with Dr. Tsuneo Ono increased my understanding on ocean chemistry. Messrs. Masahiro Watanabe and Fuyuki Saito helped me prepare the manuscript.

Some of the figures were produced with Dennou Club Library.

Contents

Chapter 1

General Introduction

1.1 Role of the oceanic ecosystem in forming the earth's climate

The biota in the ocean surface layer plays an important role in the cycling of chemical matters in the ocean including green house gases, and thus it participates in forming the climate. The "biological pump" is the most prominent of the ways it affects the climate, and its effect is readily seen in Fig. 1.1. The figure displays a vertical distribution of

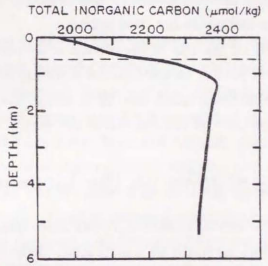

Fig. 1.1. Vertical distribution of ΣCO_2. The data were taken at GEOSECS station 214 in the North Pacific (32°N, 176°W). (adapted from Broecker and Peng, 1982)

total dissolved inorganic carbon (ΣCO_2) which can be regarded as equivalence of CO_2

in a rough sense. The profile shows a characteristic feature that ΣCO_2 concentration is significantly reduced near the sea surface. This peculiar distribution is due to effects of the ocean circulation and biological activities with the latter having the major contribution. Fig.1.2 explains the way biological activities form the profile in Fig.1.1. Dissolved inorganic carbon is uptaken by phytoplankton to form organic matters through photosynthesis in the euphotic layer ,where ample light is available for photosynthesis; after their formation, they sink out of the euphotic layer to deeper layers where they are remineralized to become inorganic carbon. The existence of these processes means that there is a sink for ΣCO_2 near the sea surface and a source in deeper layers, and thus it forms the profile in Fig.1.1. This function of the surface ecosystem to reduce ΣCO_2 is called biological pump * , and is contributing to keeping atmospheric CO_2 concentration low through gas exchange between the atmosphere and the ocean. If it were not for the pump, the equilibrium concentration of atmospheric CO_2 would be more than 1.5 times as high as the present value (*e.g.*, Shaffer, 1993).

It is important for studying this role of the ecosystem to grasp the cycling of nutrients such as phosphate and nitrate. This is because these chemical matters, which are also necessary for photosynthesis as well as inorganic carbon is, are relatively depleted in the surface layer compared with carbon itself. For this reason, many studies on the biogeochemical cycling emphasize on behavior of nutrients (*e.g.*,, Hayward, 1987; Takahashi *et al.*, 1993; and most of the modeling studies cited below).

In Section 1.2, studies on the role of the oceanic ecosystem in the biogeochemical cycling are briefly reviewed putting an emphasis on modeling studies. After clarifying their contributions as well as problems which need to be solved, the objectives of this study are stated in Section1.3 together with the contents of this thesis.

1.2 Modeling studies on the biogeochemical cycling

Along with observational efforts, numerical models have contributed to understanding of the role of the ocean biota especially on a large scale. Because of difficulties to carry out observation with satisfying resolution in time and space, numerical models can be of great help to grasp the functioning of the marine biota on a large scale.

*Also, biological activities in the surface layer affects ΣCO_2 concentration by the "alkalinity pump" which functions through formation of calcium carbonate. But its effect on the vertical change of ΣCO_2 is minor compared with that of the biological pump.

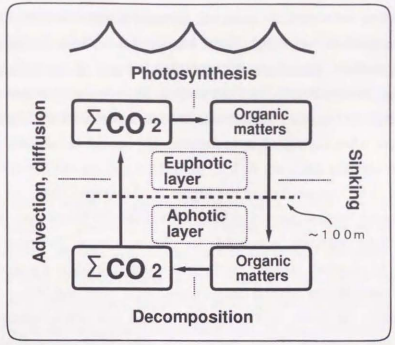

Fig. 1.2. Schematic explanation of the biological pump.

1.2.1 Models with a simplified ecosystem

Bacastow and Maier-Reimer (1990), in their pioneering work, demonstrated that overall distribution of chemical tracers including nutrients can be reproduced by incorporating the function of the biota in an extremely simple way into an ocean general circulation model (OGCM). The sinking flux of organic matters is determined as a direct function of the nutrient concentration in the uppermost layer and the solar radiation at the sea surface. Subsequently, Bacastow and Maier-Reimer (1991) and Najjar *et al.* (1992) demonstrated that the modeled distribution can be improved by including the effect of dissolved organic matters (DOM), conventionally defined as the organic matters whose size is less than 1 μm, as a mechanism of nutrient transport. In particular, DOM was shown to be effective for eliminating the unrealistic maximum of nutrient concentration at the intermediate depths in the equatorial region, which is often referred to as "nutrient trapping". Although the rich abundance of DOM reported by Sugimura and Suzuki (1988) has been corrected to smaller values by Suzuki (1993), some studies show that DOM is still significantly contributing to the biogeochemical cycling even at the modest concentration (Anderson and Sarmiento,

1995; Yamanaka, 1996). Moreover, some of these models are adopted to calculate the oceanic absorption of anthropogenic CO_2 (*cf.*, Siegenthaler and Sarmiento, 1993).

While these models have added our insight into the geochemical cycling especially in the deep or the intermediate layer, some of important features of the surface ecosystem are totally lost or only poorly treated. In these models, the ecosystem is tremendously simplified. For example, how the ecosystem responds to a change in mixed layer depth (MLD) is largely distorted; when the mixed layer deepens, the uptake of carbon by phytoplankton may be enhanced because nutrients such as phosphate and nitrate become enriched in the euphotic layer as their concentrations are higher in the deeper layer; on the other hand, it may be suppressed because phytoplankton individuals are swept away from the surface layer where the light condition is suitable for photosynthesis. Whether the increase of MLD acts to fuel or diminish primary production is determined by a subtle balance among various factors. This delicate relation between the mixed layer and biological activities can not be represented in the above mentioned models: their productions always become higher when the mixed layer deepens. This is because the effect of suppressing photosynthesis by vertical mixing is not incorporated as the components of the ecosystem like phytoplankton are not explicitly treated in those models.

1.2.2 Models with a more realistic ecosystem

A model which overcomes these defects is now desired eagerly because otherwise some of the problems which have been proposed recently can not be solved. In the North Pacific, for instance, some researchers found changes in MLD associated with the decadal climate variations and suggested their influence on the biogeochemical cycling through subsequent changes of the oceanic biota. Venrick *et al.* (1987) reported a significant increase of chlorophyll, an index of phytoplankton, in the central North Pacific. Using *in situ* data collected during 1964 - 1985, they showed that chlorophyll concentration had almost doubled during this period, though the spatial extent of the collected data (about $5° \times 5°$) is narrow. They speculated that this change is due to deepening of MLD which the decadal climate variations in the North Pacific are associated with; because surface nutrients are scarce while light is plentiful in this region, a deep MLD will stimulate phytoplankton growth by bringing nutrients up to the surface layer rather than reduce it by spoiling light condition. Polovina *et al.* (1995) showed MLD is indeed changing over the North Pacific, deepening in the subtropical gyre and shallowing in the subpolar gyre. They also suggested, using a simple ecosystem model, that the change can have an impact on biological activities, meaning that the strength of the biological pump is changing. On the other hand, Falkowski and Wilson (1992) claimed based on accumulated Secchi disk data that there is no indication of the ecosystem change on the decadal scale in the North Pacific, thereby complicating the problem. Numerical models may be powerful tools for this kind of problem, but the models discussed in Section 1.2.1 can not deal with this feature because the relation between the biological pump and the ecosystem behavior is not expressed.

An ecosystem model which can potentially treat such an issue has been developed by embedding the model of Fasham *et al.* (1990) into an OGCM. The model includes phytoplankton, zooplankton, nitrate, ammonium, particulate organic nitrogen, dissolved organic nitrogen, and bacteria. Phytoplankton in the model is vulnerable to changes in vertical mixing arising from deepening and shallowing of MLD, meaning that the effect of inhibiting photosynthesis of the deep MLD is working here. It was demonstrated by Sarmiento *et al.* (1993) and Fasham *et al.* (1993) that this model bears reasonably good results with most of the discrepancies between the model results and the observations attributed to the problems of physical environments in their OGCM.

Although the model needs many improvements in order to deal with the problems as stated above (for example, an increasing trend of surface nitrate can not be eliminated), these sorts of models have been applied to other problems. Toggweiler and Carson (1995) used the model of Sarmiento *et al.* (1993) and Fasham *et al.* (1993) in order to examine the nitrate budget in the equatorial Pacific; they speculated that the oxygen minimum lying underneath the euphotic layer in this region may be a significant sink of nitrate. Chai *et al.* (1996) also studied the equatorial Pacific by using their own model; they investigated the role of iron for maintaining the high nitrate concentration in this region, and showed that the nitrate-rich plume in the equatorial Pacific is made greatly smaller when the photosynthetic rate is doubled in the model; they state that this result has evidenced the significance of iron on maintaining the abundant nutrient in this area. Six and Maier-Reimer (1996) also developed their ecosystem model embedded in an OGCM as an extension of the model of Bacastow and Maier-Reimer (1990); they showed that the incorporation of ecosystem dynamics can improve tracer distributions by reducing the magnitude of "nutrient trapping".

1.3 Objectives and contents of this thesis

The way the ecosystem responds to changes in physical environments such as MLD is a central issue when variations of the intensity of the biological pump are investigated. The effect of the physical factors on the ecosystem is most noticeable in its seasonal variation. Changes of the ecosystem even on the decadal scale are often stated in terms of modification to seasonal features; for example, Brodeur and Ware (1993), in their paper reporting an increasing trend of zooplankton biomass in the Northeast Pacific since 1960's, inferred that reduction of photosynthesis in spring due to the deeper winter MLD may have resulted in the trend through a rather complicated process. Thus, understanding of mechanisms of the seasonal variation can provide essential comprehension of the ecosystem which varies on various time scales.

In this thesis, a model which explicitly includes ecosystem components is developed. The focus is on the seasonal variation, which in no other study with a model of this type has been throughly investigated. The North Pacific is chosen as a studying region. This is partly because various good data are available and partly because there are controversial and stimulating arguments on the decadal variation of the ecosystem (Section 1.2.2).

In Chapter 2, the ecosystem model is calibrated in the one-dimensional version. Capability to reproduce a distinct contrast between two ocean weather stations (OWSs) located in totally different oceanic regimes will be demonstrated. Implications on the dynamics of the ecosystem obtained by the simulation are also discussed. In Chapter 3, the ecosystem model calibrated in Chapter 2 is embedded in an ocean general circulation model (OGCM) for the North Pacific and results obtained by the combined model are compared with observations. This is obviously a necessary step before the model results are analyzed. Mechanisms which determine the distributions of biological variables in the model are investigated, and applicability of the mechanisms to the real ocean is discussed. Chapter 4 constitutes the central part of this thesis. It will be shown that the North Pacific can be divided into seven areas based on seasonal variation patterns and the annual mean abundance of phytoplankton. Mechanisms determining the seasonal patterns and their distribution in the model are then investigated. Chapter 5 summarizes this thesis and provides its implications on future studies on the biogeochemical cycling.

References

Anderson, L. A. and J. L. Sarmiento (1995): Global ocean phosphate and oxygen simulaions. *Glob. Biogeochem. Cycles*, **9**, 621–636.

Bacastow, R. and E. Maier-Reimer (1990): Ocean-circulation model of the carbon cycle. *Clim. Dyn.*, **4**, 95–125.

Bacastow, R. and E. Maier-Reimer (1991): Dissolved organic carbon in modeling oceanic new production. *Glob. Biogeochem. Cycles*, **5**, 71–85.

Brodeur, R. D. and D. M. Ware (1993): Interdecadal variability in distribution and catch rates of epipelatic nekton in the northeast pacific ocean. in preparation.

Broecker, W. S. and T.-H. Peng (1982): *Tracers in the Sea*, Eldigio Press, Palisades, N.Y.

Chai, F., S. T. Lindley and R. T. Barber (1996): Origin and maintenance of a high nitrate condition in the equatorial Pacific. *Deep-Sea Res. II*, **43**, 1031–1064.

Falkowski, P. G. and C. Wilson (1992): Phytoplankton productivity in the North Pacific ocean since 1900 and implications for absorption of anthropogenic CO_2. *Nature*, **358**, 741–743.

Fasham, M. J. R., H. W. Ducklow and S. M. Mckelvie (1990): A nitrogen based model of plankton dynamics in the oceanic mixed layer. *J. Mar. Res.*, **48**, 591–639.

Fasham, M. J. R., J. L. Sarmiento, R. D. Slater, H. W. Ducklow and R. Williams (1993): Ecosystem behavior at Bermuda Station S and Ocean Weather Station INDIA: an observational analysis. *Glob. Biogeochem. Cycles*, **7**, 379–415.

Hayward, T. L. (1987): The nutrient distribution and primary production in the central North Pacific. *Deep-Sea Res.*, **34**, 1593–1627.

Najjar, R. G., J. L. Sarmiento and J. R. Togweiler (1992): Downward transport and fate of organic matter in the ocean: Simulation with a general circulation model. **6**, 45–76.

Polovina, J. J., G. T. Mitchum and G. T. Evans (1995): Decadal and basin-scale variation in mixed layer depth and the impact on biological production in the Central and North Pacific, 1960-88. *Deep-Sea Res.*, **42**, 1701–1716.

Sarmiento, J. L., R. D. Slater, M. J. R. Fasham, H. W. Ducklow, J. R. Toggweiler and G. T. Evans (1993): A seasonal three-dimensional ecosystem model of nitrogen cycling in the North Atlantic euphotic zone. *Glob. Biogeochem. Cycles*, **7**, 417–450.

Shaffer, G. (1993): Effects of the marine biota on global carbon cycling. p. 431–455. In *The Global Carbon Cycle*, ed. by M. Heimann, Springer-Verlag.

Siegenthaler, U. and J. L. Sarmiento (1993): Atmospheric carbon dioxide and the ocean. *Nature*, **365**, 119–125.

Six, K. D. and E. Maier-Reimer (1996): Effects of plankton dynamics on seasonal carbon fluxes in an ocean general circulation model. *Glob. Biogeochem. Cycles*, **10**.

Sugimura, Y. and Y. Suzuki (1988): A high-temperature catallytic oxidation methods for determination of nonvolatile dissolved organic carbon in seawater by direct injection of a liquid sample. *Mar. Chem.*, **24**, 105–131.

Suzuki, Y. (1993): On the measurement of DOC and DON in seawater. *Mar. Chem.*, **41**, 287–288.

Takahashi, T., J. Olafsson, J. G. G. D. W. Chipman and S. C. Sutherland (1993): Seasonal variation of CO_2 and nutrients in the high-latitude surface oceans: A comparative study. *Glob. Biogeochem. Cycles*, **7**, 843–878.

Toggweiler, J. R. and S. Carson (1995): What are upwelling systems contributing to the ocean's carbon and nutrient budgets? Chapter 17, 337–360 In *Upwelling in the Ocean: Modern Processes and Ancient Records*, ed. by C. P. Summerhayes, K.-C. Emeis, M. V. Angel, R. L. Smith and B. Zeitzschel, John Wiley & Sons Ltd.

Venrick, E. L., J. A. McGowan, D. R. Cayan and T. L. Hayward (1987): Climate and chlorophyll a: Long-term trends in the central North Pacific Ocean. *Science*, **238**, 70–72.

Yamanaka, Y. (1996): *Development of Ocean Biogeochemical General Circulation Model*, PhD thesis, University of Tokyo.

Chapter 2

Application of the vertical one-dimensional ecosystem model to ocean weather stations in different oceanic regimes

2.1 Introduction

Primary production and subsequent processes occuring in the ocean surface layer play an important role in the biogeochemical cycling. Numerical models, together with observations, can serve to help understand the cycle. Indeed, many studies have been carried out for understanding the role of the surface biota using numerical models, most of which are on a much smaller scale than global (*e.g.*,, Doney *et al.*, 1996; Fasham *et al.*, 1990; Radach and Moll, 1993). Recently, however, the model of Fasham *et al.* (1990) was embedded in an oceanic general circulation model (OGCM) to simulate basin scale behavior of the surface biota in the North Atlantic (Sarmiento *et al.*, 1993; Fasham *et al.*, 1993). Before making such a coupling, it is obviously needed to verify the model using observations at some particular sites. Fasham *et al.* (1990) and Fasham (1993) showed that the model produces fairly good results when compared with data from Hydrostation S (32°N, 64°W) and from Ocean Weather Station (OWS) India (59°N, 19°W), respectively. It is very logical to choose those sites for testing the model because the two sites lie in the completely different oceanic regimes from each other, as is easily seen, for instance, in Levitus *et al.* (1993). Recently procedures to validate numerical models were discussed by the numerical modeling group of Joint Global Ocean Flux Study (JGOFS); there the importance to compare the numerical results and the time series data in different oceanic regimes was also pointed

out (Evans and Garçon, 1997).

Furthermore, using a box model slightly different from that mentioned above, Fasham (1995) explored the causes for the difference in seasonal variation between the North Atlantic and the North Pacific. By changing only physical conditions such as mixed layer depth (MLD) and solar radiation, he successfully reproduced the distinct contrast between these areas. His conclusion basically supports the notion of Evans and Parslow (1985) that the shallow winter mixed layer in the North Pacific prevents a bloom by maintaining the relatively large photosynthetic rate of phytoplankton even in winter. The studies referred to above, that is, Fasham *et al.* (1990), Fasham (1993), Fasham (1995), and Evans and Parslow (1985), proved that, at least within the scope of box models, a single ecosystem model can be applied to various sites if sufficient care is paid on external conditions such as MLD and light intensity. A subsequent step will be to see whether or not success can be achieved with a more complex model in which parameters prescribed in the above-mentioned models are determined internally.

In this chapter, a vertical one-dimensional ecosystem model coupled with a mixed layer model, which is also intended to be coupled with an OGCM, is applied to two OWSs, that is, OWS Papa (50°N, 145°W) and the Atlantic Time-series Study (BATS) site (*cf.*, Michaels and Knap, 1996). The oceanic regimes differ greatly in the two sites. Namely, concentrations of nutrients are far higher in the former, while chlorophyll concentration and primary production in the two sites are of the same order. This distinct contrast will enable to conduct an effective test of our model.

In this model, MLD and nutrient concentration at the bottom of the mixed layer are obtained as model output, in contrast to Fasham *et al.* (1990), Fasham (1993), and Fasham (1995), where they are given as model input. Both quantities are important for determining biological activities in the surface layer. In particular, the latter is governed by both physical and biological processes. Therefore it is still meaningful to see whether acceptable results can be obtained at different sites with this model.

In Secion 2.2, model description is given. The model is applied to OWS Papa and the BATS site in Sections 2.3 and 2.4, respectively; the model resutls are compared with observations and the implications of the model results are discussed. In Section 2.5, conclusions are provided and how the work in this chapter is related to the subsequent chapters is argued.

2.2 Model Description

Two sub-models are needed for this study; one is a mixed layer model and the other an ecosystem model. The mixed layer model adopted here is that of Kantha and Clayson (1994) who improved the Mellor and Yamada (1982)'s level 2.5 scheme. The ecosystem model is the one developed by Kawamiya *et al.* (1995), details of which are described below.

2.2.1 Description of the ecosystem model

Structure

The model is nitrogen based, and is composed of following six compartments.

- Phytoplankton (Chl)
- Zooplankton (ZOO)
- Nitrate (NO_3)
- Ammonium (NH_4)
- Particulate Organic Nitrogen (PON)
- Dissolved Organic Nitrogen (DON)

In the parentheses are their mathematical symbols. As for Particulate Organic Nitrogen and Dissolved Organic Nitrogen, symbols PON and DON, respectively, will be used as acronyms also in the text. Nitrogen based material flows are shown in Fig. 2.1.

Bacterial biomass and size distribution of planktons are neglected. This is partly due to difficulties in obtaining reliable data for constructing a model in which those effects are taken into account. The role of microbial loop cannot be explicitly included in our model; but it can be implicitly expressed by tuning zooplankton mortality because microbial loop means material flux from bacteria to zooplankton. It will be worthwhile to know to what extent this simple model can reproduce ecosystem behavior.

Formulation of each process

To obtain time evolution of the compartments, all the processes described in Fig. 2.1 have to be formulated. The following are explanation of the formulation.

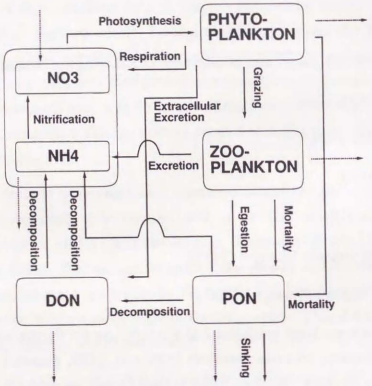

Fig. 2.1. Compartments and interactions between them in this model. Boxes represent nitrogen based standing stocks and arrows represent nitrogen flows in the ecosystem. Dashed arrows represent the exchange with deep layer through diffusion and advection.

Photosynthesis Photosynthesis is assumed to be a function of phytoplankton concentration, temperature, nutrient concentration, and intensity of light. For the dependence on nutrient concentration, Michaelis-Menten formula is adopted. Ammonium inhibition is taken into account (Wroblewski, 1977). To express the dependence on light intensity, the formula used by Steele (1962), by which light inhibition can be expressed, is employed. As for the dependence on temperature, it is assumed that photosynthetic rate is nearly doubled when temperature increases by 10°C (Eppley, 1972). Almost the same assumption is adopted for other processes that depend on temperature.

$$\begin{aligned}
(\text{Photosynthesis}) &= \\
GPP(\text{Chl}, \text{NH}_4, \text{NO}_3, T, I) &= V_{\max}\left\{\frac{\text{NO}_3}{\text{NO}_3 + K_{\text{NO3}}}\exp(-\Psi\text{NH}_4) + \frac{\text{NH}_4}{\text{NH}_4 + K_{\text{NH4}}}\right\} \\
&\times \exp(kT)\frac{I}{I_{opt}}\exp\left(1 - \frac{I}{I_{opt}}\right)\text{Chl}. \qquad (2.1)\\
I &= I_0\exp(-\Lambda|z|), \qquad (2.2)\\
\Lambda &= \alpha_1 + \alpha_2\text{Chl}. \qquad (2.3)
\end{aligned}$$

where T is temperature, z depth (positive upward and is zero at the sea surface), I light intensity, I_0 light intensity at the ocean surface, Λ light dissipation coefficient. Notation of parameters is given with their values in Table 2.1. Other parameters are also tabulated. The first term in the braces represents nitrate uptake and the second ammonium uptake. Here, the ratio of the nitrate uptake to the nitrogen uptake, R_{NO_3}, is defined as follows for the simplicity of later description.

$$R_{\text{NO}_3} = \frac{\dfrac{\text{NO}_3}{\text{NO}_3 + K_{\text{NO3}}}\exp(-\Psi\text{NH}_4)}{\dfrac{\text{NO}_3}{\text{NO}_3 + K_{\text{NO3}}}\exp(-\Psi\text{NH}_4) + \dfrac{\text{NH}_4}{\text{NH}_4 + K_{\text{NH4}}}}. \qquad (2.4)$$

Extracellular Excretion Extracellular excretion is assumed to be proportional to the photosynthesis.

$$(\text{Extracellular Excretion}) = \gamma GPP(\text{Chl}, \text{NH}_4, \text{NO}_3, T, I). \qquad (2.5)$$

Respiration of Phytoplankton In this model, the process of respiration is included although this is nitrogen based. This "respiration" does not have a counterpart in reality, but is included just to prevent the situation where net primary production has a positive

Table 2.1. Notation used in the ecosystem model and parameter values.

V_{max}	Maximum Photosynthetic Rate at 0°C	1.000	/day
k	Temperature Coefficient for Photosynthetic Rate	0.063	/°C
K_{NO3}	Half Saturation Coefficient for Inorganic Nitrogen	2.0	μmol/l
I_{opt}	Optimum Light Intensity	0.07	ly/min
α_1	Light Dissipation Coefficent of Sea Water	0.035	/m
α_2	Self Shading Coefficient	0.0281	l/μmolN m
Ψ	Ammonium Inhibition Coefficient	1.5	l/μmol
γ	Ratio of Extracellular Excretion to Photosynthesis	0.135	
R_0	Respiration Rate at 0°C	0.03	/day
k_R	Temperature Coefficient for Respiration	0.0519	/°C
M_{P0}	Phytoplankton Mortality Rate at 0°C	0.0281	l/μmolN day
k_{MP}	Temperature Coefficient for Phytoplankton Mortality	0.069	/°C
GR_{max}	Maximum Grazing Rate at 0°C	0.30	/day
k_g	Temperature Coefficient for Grazing	0.0693	/°C
λ	Ivlev Constant	1.4	l/μmolN
Chl*	Threshold Value for Grazing	0.043	μmolN/l
α	Assimilation Efficiency of Zooplankton	0.70	
β	Growth Efficiency of Zooplankton	0.30	
M_{Z0}	Zooplankton Mortality Rate at 0°C	0.0585	l/μmolN day
k_{MZ}	Temperature Coefficient for Zooplankton Mortality	0.0693	/°C
V_{PI0}	PON Decomposition Rate at 0°C (to Inorganic Nitrogen)	0.030	/day
V_{PIT}	Temperature Coefficient for PON Decomposition (to Inorganic Nitrogen)	0.0693	/°C
V_{PD0}	PON Decomposition Rate at 0°C (to DON)	0.030	/day
V_{PDT}	Temperature Coefficient for PON Decomposition (to DON)	0.0693	/°C
V_{DI0}	DON Decomposition Rate at 0°C	0.030	/day
V_{DIT}	Temperature Coefficient for DON Decompotion	0.0693	/°C
k_{N0}	Nitrification Rate at 0°C	0.030	/day
k_{NT}	Temperature Coefficient for Nitrification	0.0693	/°C
W	Vertical Current Velocity	0.36	m/yr

Table 2.2. Parameters different between the simulations of OWS Papa and the BATS site.

		Papa	BATS	
K_{NO_3}	Half saturation constant for nitrate	2.0	0.03	μmol/l
K_{NH_4}	Half saturation constant for ammonium	0.6	0.1	μmol/l
S	Sinking velocity of PON*	$20 \sim 100$	6.5	m/day

*The sinking velocity is allowed to vary with depth at OWS Papa.

sign even at a depth which is obviously below the compensation depth. The same kind of process is also included in the model of Horiguchi and Nakata (1995).

"Respiration" of phytoplankton is assumed to be proportional to phytoplankton concentration and be dependent on temperature. Then, respiration can be expressed as follows;

$$(\text{Respiration of Phytoplankton}) = R_0 \exp(k_R T)\text{Chl}. \tag{2.6}$$

The parameter value for this "respiration" is assumed to be about the same as the real respiration.

Mortality Following Steele and Henderson (1992), mortality of phytoplankton and zooplankton is assumed to be proportional to the second power of plankton concentrations and be dependent on temperature. That is:

$$(\text{Mortality of Phytoplankton}) = MP_0 \exp(k_{MP} T)\text{Chl}^2; \tag{2.7}$$

$$(\text{Mortality of Zooplankton}) = MZ_0 \exp(k_{MZ} T)\text{ZOO}^2. \tag{2.8}$$

Grazing Grazing is expressed as a function of temperature, phytoplankton concentration, and zooplankton concentration.

$$\begin{aligned}(\text{Grazing}) &= \\ GR(T, \text{Chl}, \text{ZOO}) &= \text{Max}\left\{0, GR_{\max} \exp(k_g T)\{1 - \exp(\lambda(\text{Chl}^* - \text{Chl}))\}\text{ZOO}\right\},\end{aligned} \tag{2.9}$$

where Max$\{a,b\}$ equals to the larger one of a and b. In this formulation, grazing rate is saturated when phytoplankton concentration is sufficiently large, while no grazing occurs when phytoplankton concentration is lower than the critical value (Chl*).

Excretion and Digestion by Zooplankton Excretion and Digestion are assumed to be proportional to grazing.

$$(\text{Excretion}) = (\alpha - \beta) GR(T, \text{Chl}, \text{ZOO}), \tag{2.10}$$

$$(\text{Digestion}) = (1 - \alpha) GR(T, \text{Chl}, \text{ZOO}). \tag{2.11}$$

Decomposition of Organic Matters, Nitrification Decomposition rates of PON and DON and nitrification rate are assumed to depend on temperature. Thus,

$$\begin{aligned}
(\text{Decomposition of PON into Ammonium}) &= V_{PI0}\exp(V_{PIT}T)\text{PON} && (2.12)\\
(\text{Decomposition of PON into DON}) &= V_{PD0}\exp(V_{PDT}T)\text{PON} && (2.13)\\
(\text{Decomposition of DON into Ammonium}) &= V_{DI0}\exp(V_{DIT}T)\text{DON} && (2.14)\\
(\text{Nitrification}) &= k_{N0}\exp(k_{NT}T)\text{NH}_4. && (2.15)
\end{aligned}$$

In many models, it is assumed that, unlike in this one, nitrification does not occur in the mixed layer. But Ward (1987) suggested that vigorous nitrification occurs near the bottom of the mixed layer, where significant photosynthesis is still occurring. It is not very unrealistic to assume that modest nitrification is occurring throughout the water column.

Vertical Diffusion and Advection Letting C_i be one of the compartments in this model, effects of vertical diffusion($\text{Dif}(C_i)$) and advection($\text{Adv}(C_i)$) are formulated as follows;

$$\begin{aligned}
\text{Dif}(C_i) &= \frac{\partial}{\partial z}\left(K_V\frac{\partial C_i}{\partial z}\right), && (2.16)\\
\text{Adv}(C_i) &= -W\frac{\partial C_i}{\partial z}, && (2.17)
\end{aligned}$$

where K_V is the vertical diffusion coefficient, and W vertical current velocity. For all compartments the same K_V is adopted assuming that phytoplankton and zooplankton are subject to mixing in exactly the same way as passive tracers are. The values of vertical velocity are specified externally as stated in Section 2.2.2.

Sinking of PON Letting S be sinking velocity of PON, sinking of PON can be written in the form,

$$(\text{Sinking of PON}) = -\frac{\partial}{\partial z}(S\cdot\text{PON}). \qquad (2.18)$$

Governing Equations

Combining those processes formulated, how each compartment evolves with time t can be described as follows.

$$\begin{aligned}
\frac{d\text{NO}_3}{dt} &= -\{(\text{Photosynthesis})-(\text{Respiration})\}R_{\text{NO}_3}\\
&\quad + (\text{Nitrification}) + \text{Dif}(\text{NO}_3) + \text{Adv}(\text{NO}_3) && (2.19)\\
\frac{d\text{NH}_4}{dt} &= -\{(\text{Photosynthesis})-(\text{Respiration})\}(1-R_{\text{NO}_3})\\
&\quad - (\text{Nitrification}) + (\text{Decomposition of PON into Ammonium})\\
&\quad + (\text{Decomposition of DON into Ammonium}) + (\text{Excretion})\\
&\quad + \text{Dif}(\text{NH}_4) + \text{Adv}(\text{NH}_4) && (2.20)\\
\frac{d\text{Chl}}{dt} &= (\text{Photosynthesis}) - (\text{Extracellular Excretion})\\
&\quad - (\text{Mortality of Phytoplankton}) - (\text{Grazing})\\
&\quad + \text{Dif}(\text{Chl}) + \text{Adv}(\text{Chl}) && (2.21)\\
\frac{d\text{PON}}{dt} &= (\text{Mortality of Phytoplankton}) + (\text{Mortality of Zooplankton})\\
&\quad + (\text{Digestion}) + (\text{Sinking of PON})\\
&\quad - (\text{Decomposition of PON into Ammonium})\\
&\quad - (\text{Decomposition of PON into DON})\\
&\quad + \text{Dif}(\text{PON}) + \text{Adv}(\text{PON}) && (2.22)\\
\frac{d\text{DON}}{dt} &= (\text{Extracellular Excretion})\\
&\quad + (\text{Decomposition of PON into DON})\\
&\quad - (\text{Decomposition of DONintoammonium})\\
&\quad + \text{Dif}(\text{DON}) + \text{Adv}(\text{DON}) && (2.23)\\
\frac{d\text{ZOO}}{dt} &= (\text{Grazing}) - (\text{Digestion}) - (\text{Excretion})\\
&\quad - (\text{Mortality of Zooplankton})\\
&\quad + \text{Dif}(\text{ZOO}) + \text{Adv}(\text{ZOO}) && (2.24)\\
& && (2.25)
\end{aligned}$$

Parameters

The parameter values are given in Table 2.1. Some of them are different between the simulations of OWS Papa and the BATS site. Such values are displayed in Table 2.2 separately. Readers can be referred to Kawamiya *et al.* (1995) and Kawamiya *et al.* (1997) on the choice of these values.

Between the two sites, the half saturation constants for nitrate and ammonium are changed rather dramatically by order(s) of magnitude. This change can be justified because

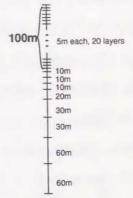

Fig. 2.2. Grid intervals.

the two are located in very different oceanic regimes, *i.e.*, OWS Papa is in a eutrophic region and the BATS site in an oligotrophic region. This constant is known to be far smaller in the oligotrophic than in the eutrophic region (*e.g.*, Eppley *et al.*, 1969; Parsons *et al.*, 1984; Harrison *et al.*, 1996). Also, the larger sinking velocity of particulate organic nitrogen (PON) in OWS Papa is qualitatively justified due to the fact that the subpolar region is dominated by relatively large phytoplankton compared with the subtropical region (*e.g.*, Ishizaka *et al.*, 1994).

2.2.2 Settings

The domain extends to the depth of 330 m and is divided into 28 levels; the grid intervals are 5 m in the upper 100 m then become gradually larger with depth to 60 m in the bottom layer (Fig. 2.2).

Boundary conditions are as follows:

- Top

  Temperature and salinity are fixed to time-dependent observational values; specific ways of imposing them are different between the two locations and will be explained later. Wind stresses are calculated from objective analysis data provided by European Centre for Medium-Range Weather Forecasts (ECMWF) whose time interval is twelve hours. Ecological variables are not allowed to be exchanged between the atmosphere and the ocean.

- Bottom

Table 2.3. Boundary conditions at the bottom of the model($z = -330$ m). The Value for nitrate was taken from Levitus *et al.* (1993).

	Papa	BATS
Temperature(°C)	4.5	18.0
Salinity(psu)	33.91	36.55
Phytoplankton(μmolN/l)	0	0
Zooplankton(μmolN/l)	0	0
Ammonium(μmol/l)	0	0
Nitrate(μmol/l)	37	4

  Temperature, salinity, and ecological variables except PON and DON are fixed to constant values close to observational ones (Table 2.3), while it is assumed that PON and DON have no vertical gradient. Horizontal velocities in the mixed layer model is fixed to zero.

The background viscosity for the mixed layer model is set to 1cm^2/sec at both locations, while the diffusivity is 0.3 cm^2/sec at OWS Papa and 1 cm^2/sec at the BATS site. The larger diffusivity at the BATS site is justified by Musgrave *et al.* (1988) and Spitzer and Jenkins (1989) who argued that this large value is needed for a realistic simulation of chemical tracers near Bermuda.

The vertical profile and the temporal variation of vertical current velocity are specified in the following way; the absolute values of vertical velocity become largest at the depth of 30m (Price *et al.*, 1987) then linearly become smaller as the depths get either shallower or deeper, so that they vanish at the top and the bottom of the domain; the maximum values are prescribed using cosine curves so that they fit the Ekman velocities derived from the dataset of Hellerman and Rosenstein (1983), that is,

$$W_{30} = W_{\text{mean}} + W_{\text{amp}} \cos\left(\frac{2\pi F}{Y} t\right), \tag{2.26}$$

where W_{30} is the vertical velocity at 30 m depth, W_{mean} its annual mean, W_{amp} its amplitude of seasonal variation, Y a constant whose value is 1 year, F the number of oscillation per year. The values of W_{mean}, W_{amp}, and F are given in Table 2.4.

Diurnal variation of solar radiation is incorporated following Ikushima (1967);

$$I_0 = \text{Max}\{I_{0\text{max}} \sin^3((\pi/D)t), 0\} \tag{2.27}$$

Table 2.4. Parameter values for the vertical velocity at OWS Papa and the BATS site.

	Papa	BATS
W_{mean} (m day^{-1})	0.064	-0.16
W_{amp} (m day^{-1})	-0.043	-0.095
F	2	1

where $I_{0\text{max}}$ is the maximum light intensity at the sea surface and D the day length which is calculated using an astronomical formula. The values of $I_{0\text{max}}$ are calculated from monthly mean radiation ($I_{0\text{mean}}$) given by Oberhuber (1988) using the following equation:

$$I_{0\text{max}} \int_{t=0}^{t=24\text{hour}} \text{Max}\left\{\sin\left(\frac{2\pi}{D}t\right), 0\right\} dt = I_{0\text{mean}}. \tag{2.28}$$

Initial conditions and time integration are different between the two sites, and will be described separately in later sections corresponding to each station.

2.3 Simulation at OWS Papa

In this section, model results for OWS Papa are compared with corresponding observations. Implications obtained from the comparison are discussed.

2.3.1 Time integration and results of the mixed layer model

The initial values for temperature and salinity are taken from the average vertical profiles observed in 1980. Initial values of horizontal velocities are set to be zero everywhere. Temperature and salinity imposed at the sea surface are also taken from the data in 1980. Boundary conditions at the bottom are given in Table 2.3. The year 1980 is chosen because of availability of the good data.

Integration is performed for two years from January 1 under the cyclic forcing of 1980. Fig. 2.3 shows the seasonal variation of temperature in the second year of the model and that from the observation. The model and the observation show overall agreement.

Temperature and the diffusion coefficient obtained during the second year are used in the ecosystem model.

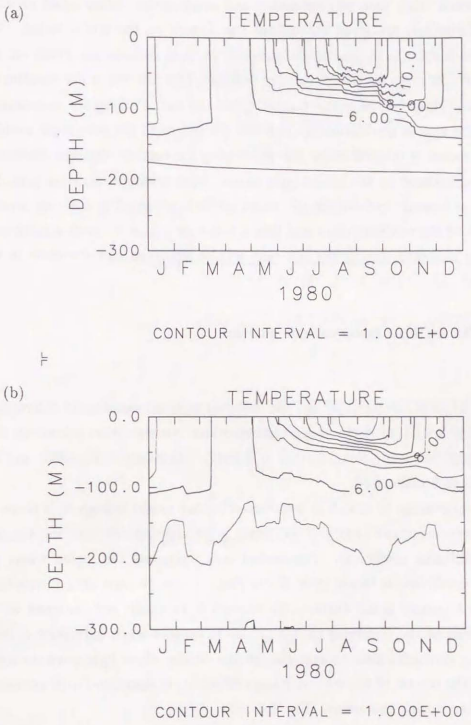

Fig. 2.3. Seasonal variation of temperature at OWS Papa in 1980 for (a) the model and (b) the observation. 31-day running averaged data are used for the observation. The unit is in °C.

2.3.2 Time integration of the ecosystem model

For the compartments other than phytoplankton and zooplankton, values equal to those at the bottom (Table 2.3) are given throughout the domain as the initial values. For phytoplankton and zooplankton, characteristic values for each variable are given; for the former, 0.15 μmolN/l is given for 0~120 m , and 0 μmolN/l for the rest of the domain; for the latter, 0.4 μmolN/l for 0~120 m and 0 μmolN/l for the rest. Preliminary experiments showed that there is almost no dependence on initial conditions in the ecosystem model.

The ecosystem model is integrated for 101 years using the vertical diffusion coefficient and temperature calculated by the mixed layer model. Such a long integration period is necessary to achieve a steady cycle of nitrate, whose profile is governed by diffusion process in the deeper part of the model domain and thus needs a long time to reach a stationary state. The results obtained during the last year will be displayed and discussed in the following sections.

2.3.3 Results of the ecosystem model

chlorophyll

Figs. 2.4(a) and (b) show the modeled and the observed seasonal variation of chlorophyll, respectively. In Fig.2.4(a), nitrogen based phytoplankton concentration is converted to chlorophyll concentration using the C:N ratio of 133:17 (Takahashi *et al.*, 1985) and the common C:Chlorophyll ratio of 50.

The maximum appearing in March is reproduced by the model though it is more intensive. Fig. 2.5 demonstrates that this maximum is strongly related with the seasonal variation of the diffusion coefficient. The shaded area represents the region where the vertical diffusion coefficient is larger than 10 cm^2/sec. It can be seen that phytoplankton concentration increases as the shaded area retreats in February, and decreases as the shaded area deepens at the beginning of April. This is because when diffusivity is large, it is impossible for phytoplankton to aggregate to the depths where light environment is suitable. In turn, the retreat of the area with large diffusivity is associated with weakening of the imposed wind during this period (Fig. 2.6).

In summer, a weak subsurface chlorophyll maximum (SCM) appears in the model. This SCM is formed due to the light inhibition. The light environment is best for phytoplankton at these depths. The SCM can be seen also in the observation.

(a)

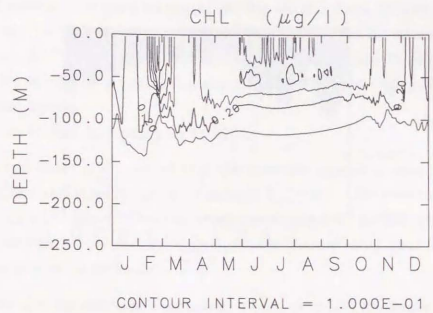

(b)

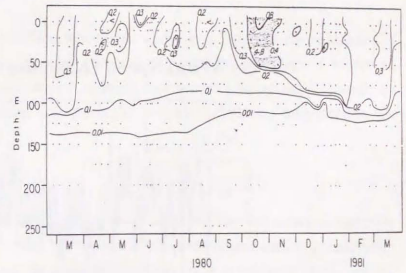

Fig. 2.4. Seasonal variation of chlorophyll for (a) the model and (b) the observation. The figure for the observation is redrawn from Clemons and Miller (1984). The unit is in μg/l.

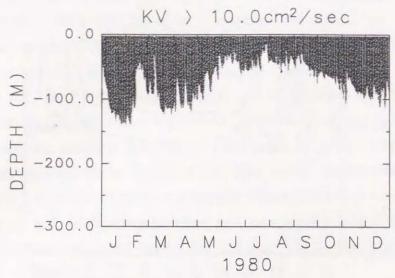

Fig. 2.5. Seasonal variation of the diffusion coefficient. The shaded area indicates where $K_V > 10$ cm^2/sec.

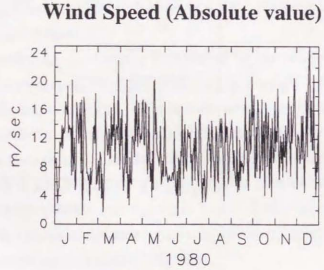

Fig. 2.6. Seasonal variation of wind speed ($= (u^2 + v^2)^{1/2}$ where u and v represent the eastward and the northward wind velocity, respectively) at OWS Papa.

The model can not reproduce the maximum that appears from fall to winter in Fig. 2.4(b). Fall phytoplankton maxima are often related to the enhanced vertical mixing and the subsequent increase of nutrient concentration. But at OWS Papa, nutrient concentration is always high (~ 10 μmol/l) compared with the observed half saturation constants (Anderson *et al.*, 1977). Thus, contribution of the enhanced mixing to phytoplankton growth cannot be so large as to form the maximum. Reasons for the discrepancy must be sought from other aspects.

Possible reasons for this discrepancy are as follows:

- Clemons and Miller (1984) report that the dominant species changes in fall and photosynthetic rate is still around the maximum in October while the solar radiation is decreasing in this season. Thus, one possible explanation for the discrepancy is that seasonal variation of species compositions (namely seasonal variation of parameters) is not incorporated in the model.

- It is known that the dominant zooplankton species move into the deeper place (say, below 250 m) at about the end of August to prepare for spawning (Miller *et al.*, 1984). Thus, another explanation for the discrepancy is that the life history of zooplankton is neglected in the model.

Incorporation of one/both of the effects mentioned above may improve the matching of the model with the observation. However, because the main purpose here is to see to what extent this general model can reproduce ecosystem behavior at certain locations, no further improvement has been added concerning this problem, which may be related to the features specific to this location.

Nitrate

Figs. 2.7(a) and (b) show, respectively, the modeled and the observed seasonal variation of nitrate. The model does reproduce the feature that nitrate concentration is extremely high throughout the year although the gradient of the nitracline is less steep in the model. It also yields the minimum in fall, just before the winter mixing brings up nitrate from the underlying layer.

The cause for the maintenance of the high nitrate concentration at OWS Papa is often argued. Ammonium inhibition can be a candidate but plays only a minor role; the ammonium inhibition factor ($\exp\{-\Psi \mathrm{NH_4}\}$ in Eq. (2.1)) has a value of only ~ 0.75 taking

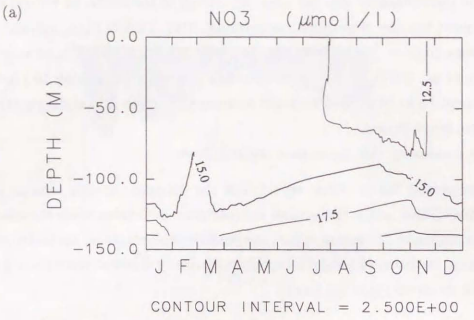

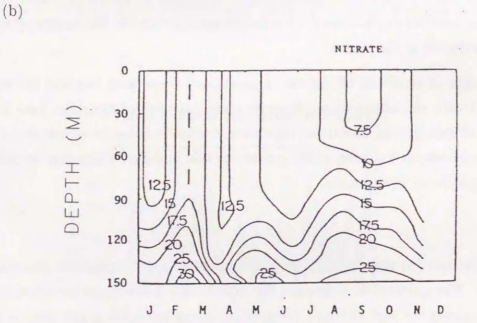

Fig. 2.7. Seasonal variation of nitrate for (a) the model and (b) the observation. The figure for the observation shows the seasonal variation averaged over years, and is redrawn from Anderson *et al.* (1977)

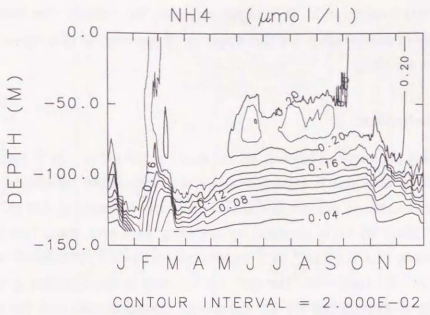

Fig. 2.8. Seasonal variation of ammonium obtained by the model.

0.2 μmol/l as a characteristic concentration of ammonium (Fig.2.8). Changing the parameter value for photosynthesis by this amount does not affect the simulated order of nitrate concentration (Kawamiya, 1994). In this model, the ultimate cause is that nitrate concentration is extraordinarily high in the deep layer. Due to the high concentration in the deep layer, nitrate is supplied vigorously by diffusion even when its concentration is high at the sea surface; phytoplankton can not spend up the nitrate because constraint from grazing pressure becomes large before phytoplankton increases enough to do so.

It is often said that high nitrate concentration may be due to iron limitation. But the value of maximum photosynthetic rate ($V_{\max}$) used in this model is not lower than the values found in the subtropical gyre where iron limitation is said to be not working; this implies that iron limitation is not considered in our model. Thus, the result of our model suggests that iron limitation is not necessarily essential for maintaining the high nitrate concentration.

It can not be said, however, from the model result that iron is playing no role in the

marine ecosystem. What the result shows is that the high nutrient concentration and the low chlorophyll concentration are not necessarily incompatible even if the iron limitation is not taken into consideration. It is highly probable, for example, that iron is playing an important role in determining the size structure of plankton in this region (Morel *et al.*, 1991; Price *et al.*, 1991).

Primary production

Annual primary production obtained by the model is 128 gC m^{-2} yr^{-1} (using a C:N ratio of 133:17), 28 % of which is exported across the 100m depth by sinking of PON. The calculated production is not much different from the estimate of 140 gC m^{-2} yr^{-1} by Wong *et al.* (1995) which is obtained by averaging data over years, but is rather lower than the estimate of 170 gC m^{-2} yr^{-1} by Welschmeyer *et al.* (1993) which is based on the observations in 1987 and 1988. The agreement is satisfactory considering that the model is not capable of reproducing the fall chlorophyll maximum and that the main objective here is just to see whether the model can bear the distinct contrast between OWS Papa and the BATS site.

2.4 Simulation at the BATS site

The model is next applied to the BATS site. This site has a very low nitrate concentration but the comparable chlorophyll concentration and the annual production to those of OWS Papa. The main interest here is reproduction of this apparently incoherent situation.

2.4.1 Time integration and results of the mixed layer model

Four simulations are made separately for the years 1989-1992. Taking the initial conditions from annual mean profiles of temperature and salinity, each integration is started on November 24 in the previous year. Temperature and salinity data for the surface boundary conditions are taken from the World Wide Web (WWW) site of the BATS project (URL: http://www.bbsr.edu/bats/). Boundary conditions at the bottom are given in Table 2.3.

The mean temperature for the four years of the seasonal cycle calculated by the model is displayed in Fig.2.9(a). Fig.2.9(b) shows the climatological cycle of temperature for 1961-1970 at Hydrostation S (32°N, 64°W) located very close to the BATS site. The model

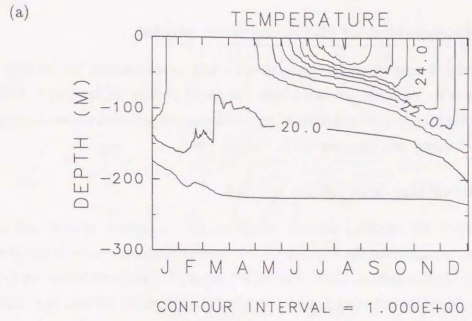

Fig. 2.9. (a) Seasonal variation of temperature at the BATS site (31°N, 64°W) averaged over the years 1989-1992 for the mixed layer model and (b) Climatological (1961-1970) seasonal variation of temperature for Hydrostation S (32°N, 64°W). (b) is adapted from Doney *et al.* (1996). The unit is in °C.

result grasps the features in the observation such as the occurrence of the relatively deep convection in February.

2.4.2 Time integration of the ecosystem model

The ecosystem model is also separately integrated for four years starting on January 1. The initial conditions for each run are taken from the model profiles on January 1, which are picked up from the steady cycle obtained by an preliminary experiment under the cyclic usage of vertical diffusivity and temperature in the year 1989.

2.4.3 Results of the ecosystem model

Figs. 2.10 - 2.12 show the modeled seasonal variations for chlorophyll, nitrate, and net primary production averaged over the four years; the corresponding observation is also given (Doney *et al.*, 1996). In this section, the C:N and C:Chlorophyll ratios used in Section 2.3.3 are again adopted. Some characteristic features seen in the observation are well reproduced in the model, *i.e.*, the high abundance of chlorophyll in winter season throughout the water column, the deep chlorophyll maximum in summer at the depths of the nitracline, the nitrate depletion in the surface layer, and the extraordinarily large primary production in early spring. The high chlorophyll concentration and primary production in late February are, like the chlorophyll maximum in March at OWS Papa, due to the retreat of the mixed layer. However, this shallowing of the mixed layer is a result of surface warming instead of weakening of the wind. Strengths of the wind at the BATS site are <5 m/sec for most of the integration period and are not so strong as to create a large variation in the MLD (as shown in Fig. 2.6, typical wind speed at OWS Papa is much stronger than that at the BATS site).

Modeled annual primary production averaged over the four years is 115 gC m^{-2} yr^{-1}. This is in good agreement with the estimate of 110 $\sim$ 140 gC m^{-2} yr^{-1} by Lohrenz *et al.* (1992).

3.7 % of the total annual primary production is exported across the 150m level by the sinking of PON. This value can be directly compared with data from sediment traps, and turned out to be lower but not very much different from the observational value of 5-7 % by Michaels and Knap (1996).

Although the model results showed basically good agreement with the observations, a closer look can of course reveal some differences between the model results and the

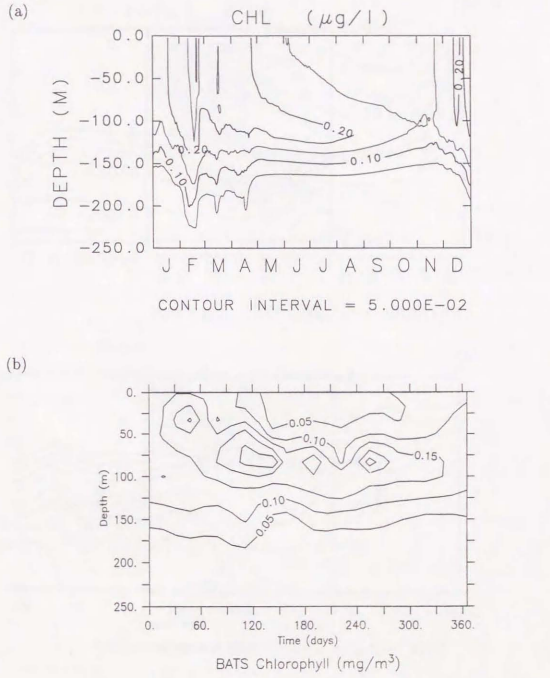

Fig. 2.10. Seasonal variation of chlorophyll for (a) the model and (b) the observation (redrawn from Doney *et al.*, 1996). The observation is for the BATS site.

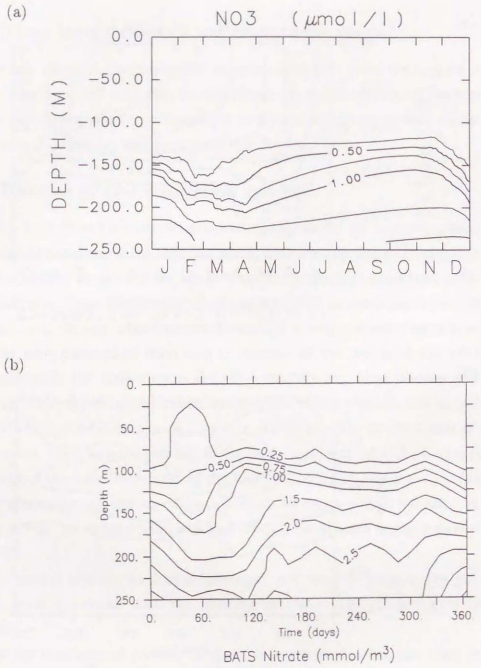

Fig. 2.11. Same as Fig.2.10 but for nitrate. Contour intervals are 0.25 μmol/l for the range of 0.0-1.0 μmol/l, and 0.5 μmol for >1.0 μmol/l.

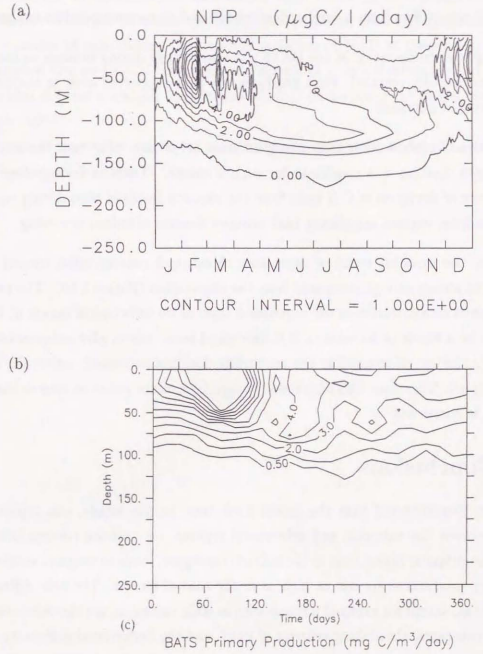

Fig. 2.12. Same as Fig.2.10 but for net primary production.

observations. For example, most vigorous production in the model occurs at the bottom of the euphotic zone in summer, while the observations show that primary production is higher in the upper portion of the euphotic zone in this season. The model of Doney *et al.* (1996) also suffers from a similar discrepancy and gives some possible explanations:

- The species composition at the BATS site may change during summer so that nutrients are rapidly recycled. High production is thus supported even at the extremely low level of nutrients.
- A source of nitrate other than transport from below may exist near the sea surface. Nitrogen fixation is a candidate for such a source. There is strong observational evidence of deviation of C:N ratio from the common Redfield ratio during summer in oligotrophic regions, suggesting that nitrogen fixation is indeed occurring.

Moreover, the modeled trend of decreasing chlorophyll concentration toward the sea surface is not strong enough compared with the observation (Figure 2.10). The extremely low chlorophyll concentration in the uppermost layer of the subtropical region is, however, believed to be a result of increase in N/Chlorophyll ratio due to photoadaptation (Winn *et al.*, 1996); the low chlorophyll at the sea surface does not necessarily reflect the decrease of biomass itself. Therefore, this discrepancy might be a minor defect as long as the cycling of nitrogen is concerned.

2.5 Conclusions

It has been demonstrated that the model used here, on the whole, can reproduce the contrast between the subpolar and subtropical regions, *i.e.*, nitrate concentration is far higher in the subpolar region than in the subtropical region, while chlorophyll concentration and primary production are not as high as in the case of nitrate. The only differences in model settings, except for external forcings such as solar radiation, are the values of the half saturation constants, the sinking velocity of PON, and the background diffusivity. Each of the difference has some supporting evidence from observational or modeling efforts. The model is shown to be able to yield reasonable results for very different oceanic regimes with appropriate choices of the parameters.

In the next chapter, the ecosystem model is combined with an OGCM. Because it is very difficult to directly incorporate spatial variations of the parameters, a suitable set

for the values of the parameters will be sought again on the spatial scale of the model domain which is far larger than that considered in this chapter. This strategy is somewhat like that adopted in embedding a bulk mixed layer model in an OGCM; first, a bulk mixed layer model is tested at a couple of specific locations; after demonstrating that the model is capable of reproducing the seasonal variation of MLD at these sites, the model is incorporated into an OGCM with some modifications in model structure and parameter values so that it bears a realistic distribution of MLD on a scale of the model domain (*e.g.*, Oberhuber, 1993).

The choice of parameter values for embedding the ecosystem model in an OGCM and its justification will be given in Chapter 3.

References

Anderson, G. C., R. K. Lam, B. C. Booth and J. M. Glass (1977): A description and numerical analysis of the factors affecting the processes of production in the Gulf of Alaska. University of Washington, Department of Oceanography Special Report 76 (Reference M-77-40) 231 pp.

Clemons, M. J. and C. B. Miller (1984): Blooms of large diatoms in the oceanic, subarctic Pacific. *Deep-Sea Res.*, **31**, 85–95.

Doney, S. C., D. M. Glover and R. G. Najjar (1996): A new coupled, one-dimensional biological-physical model for the upper ocean: Applications to the JGOFS Bermuda Atlantic Time-series Study (BATS) site. *Deep-Sea Res. II*, **43**, 591–624.

Eppley, R. W. (1972): Temperature and phytoplankton growth in the sea. *Fish. Bull.*, **70**, 1063–1085.

Eppley, R. W., J. N. Rogers and J. J. McCarthy (1969): Half saturation constants for uptake of nitrate and ammonium by marine phytoplankton. *Limnol. Oceanogr.*, **14**, 912–920.

Evans, G. T. and V. C. Garçon eds. (1997): *JGOFS Report No. 23, One-Dimensional Models of Water Column Biogeochemistry*, International Council of Scientific Unions.

Evans, G. T. and J. S. Parslow (1985): A model of annual plankton cycles. *Biological Oceanography*, **3**, 327–347.

Fasham, M. J. R. (1993): Modelling the marine biota. p. 457–504. In *The Global Carbon Cycle*, ed. by M. Heimann, Springer-Verlag.

Fasham, M. J. R. (1995): Variations in the seasonal cycle of biological production in subarctic oceans: A model sensitivity analysis. *Deep-Sea Res.*, **42**, 1111–1149.

Fasham, M. J. R., H. W. Ducklow and S. M. Mckelvie (1990): A nitrogen based model of plankton dynamics in the oceanic mixed layer. *J. Mar. Res.*, **48**, 591–639.

Fasham, M. J. R., J. L. Sarmiento, R. D. Slater, H. W. Ducklow and R. Williams (1993): Ecosystem behavior at Bermuda Station S and Ocean Weather Station INDIA: an observational analysis. *Glob. Biogeochem. Cycles*, **7**, 379–415.

Harrison, W. G., L. R. Harris and B. D. Irwin (1996): The kinetics of nitrogen utilization in the oceanic mixed layer: Nitrate and ammonium interactions at nanomolar concentrations. *Limnol. Oceanogr.*, **41**, 16–32.

Hellerman, S. and M. Rosenstein (1983): Normal monthly wind stress over the world ocean with error estimates. *J. Phys. Oceanogr.*, **13**, 1093–1104.

Horiguchi, F. and K. Nakata (1995): Water quality analysis of Tokyo Bay using mathematical model. *J. Adv. Mar. Sci. Tech. Soci.*, **1**, 71–92, in Japanese with English abstract.

Ikushima, I. (1967): Ecological studies on the productivity of aquatic plant cmmunities. III effect of depth on daily photosynthesis in submerged macrophtes. *Bot. Mag.*, **80**, 57–67.

Ishizaka, J., H. Kiyosawa, K. Ishida, K. Ishikawa and M. Takahashi (1994): Meridional distribution and carbon biomass of autotrophic picoplankton in the Central North Pacific Ocean during Late Northern Summer 1990. *Deep-Sea Res.*, **41**, 1745–1766.

Kantha, L. H. and C. A. Clayson (1994): An improved mixed layer model for geophysical applications. *J. Geophys. Res.*, **99**, 25,235–25,266.

Kawamiya, M. (1994): Modeling of the oceanic ecosystem: sensitivity experiments and application of the model. Master's thesis, University of Tokyo, In Japanese.

Kawamiya, M., M. J. Kishi, Y. Yamanaka and N. Suginohara (1995): An ecological-physical coupled model applied to Station Papa. *J. Oceanogr.*, **51**, 635–664.

Kawamiya, M., M. J. Kishi, Y. Yamanaka and N. Suginohara (1997): Obtaining reasonable results in different oceanic regimes with the same ecological-physical coupled model. *J. Oceanogr.*, **in press**.

Levitus, S., M. E. Conkright, J. L. Reid, R. G. Najjar and A. Mantyla (1993): Distribution of nitrate phosphate and silicate in the world oceans. *Prog. Oceanog.*, **31**, 245–273.

Lohrenz, S. E., G. A. Knauer, V. L. Asper, M. Tuel, A. F. Michaels and A. H. Knap (1992): Seasonal variability in primary production and particle flux in the northwestern Sargasso Sea: U. S. JGOFS Bermuda Atlantic time-series study. *Deep-Sea Res.*, **39**, 1373–1391.

Mellor, G. L. and T. Yamada (1982): Development of a turbulence closure model for geophysical fluid problems. *Rev. Geophys. Space Phys.*, **20**, 851–875.

Michaels, A. F. and A. H. Knap (1996): Overview of the U.S.JGOFS Bermuda Atlantic Time-series Study and the Hydrostaion S program. *Deep-Sea Res. II*, **43**, 157–198.

Miller, C. B., B. W. Frost, H. P. Batchelder, M. J. Clemons and R. E. Conway (1984): Life histories of large, grazing copepods in a subarctic ocean gyre: *Neocalanus plumchrus, Neocalanus cristatus*, and *eucalanus bungii* in the norhteast Pacific. *Prog. Oceanog.*, **13**, 201–243.

Morel, F. M. M., J. G. Rueter and N. M. Price (1991): Iron nutrition of phytoplankton and its possible importance in the ecology of ocean regions with high nutrients and low biomass. *Oceanography*, **4**, 56–61.

Musgrave, D. L., J. Chou and W. J. Jenkins (1988): Application of a model of upper-ocean physics for studying seasonal cycles. *J. Geophys. Res.*, **93**, 15,679–15,700.

Oberhuber, J. M. (1988): An atlas based on the 'COADS' data set: The budgets of heat, buoyancy and turbulent kinetic energy at the surface of the global ocean. Technical Report 15, Max-Planck-Institut für Meteorologie.

Oberhuber, J. M. (1993): Simulation of the Atlantic circulation with a coupled sea ice - mixed layer - isopycnal general circulation model. Part I. *J. Phys. Oceanogr.*, **22**, 808–829.

Parsons, T. R., M. Takahashi and B. Hargrave (1984): *Biological Oceanographic Processes*, Pergamon Press, 3rd edition.

Price, J. F., R. A. Weller and R. R. Schudlich (1987): Wind-driven ocean currents and Ekman transport. *Science*, **238**, 1534–1538.

Price, N. M., L. F. Andersen and F. M. M. Morel (1991): Iron and nitrogen utilisation of equatorial Pacific plankton. *Deep-Sea Res.*, **1991**, 1361–1378.

Radach, G. and A. Moll (1993): Estimation of the variability of production by simulating annual cycles of phytoplankton in the central North Sea. *Prog. Oceanog.*, **31**, 339–419.

Sarmiento, J. L., R. D. Slater, M. J. R. Fasham, H. W. Ducklow, J. R. Toggweiler and G. T. Evans (1993): A seasonal three-dimensional ecosystem model of nitrogen cycling in the North Atlantic euphotic zone. *Glob. Biogeochem. Cycles*, **7**, 417–450.

Spitzer, W. S. and W. J. Jenkins (1989): Rates of vertical mixing, gas exchange and new production: Estimates from seasonal gas cycles in the upper ocean. *J. Mar. Res.*, **47**, 169–196.

Steele, J. H. (1962): Environmental control of photosynthesis in sea. *Limnol. Oceanogr.*, **7**, 137–150.

Steele, J. H. and E. W. Henderson (1992): The role of predation in plankton models. *J. Plankton Res.*, **14**, 157–172.

Takahashi, T., W. S. Broecker and S. Langer (1985): Redfield ratio based on chemical data from isopycnal surfaces. *J. Geophys. Res.*, **90**, 6907–6924.

Ward, B. B. (1987): Nitrogen transformations in the Southern California Bight. *Deep-Sea Res.*, **34**, 785–805.

Welschmeyer, N. A., S. Storm, R. Goericke, G. DiTullio, M. Belvin and W. Petersen (1993): Primary production in the Subarctic Pacific Ocean: Project SUPER. *Prog. Oceanog.*, **32**, 101–135.

Winn, C. C., R. M. L. C. Campbell, J. R. Christian, D. V. Hebel, J. E. Dore, L. Fujieki and D. M. Karl (1996): Seasonal variability in the phytoplankton community of the North Pacific Subtropical Gyre. *Glob. Biogeochem. Cycles.* **9**, 605–620.

Wong, C. S., A. A. Whitney, K. Iseki and J. S. Page (1995): Analysis of trends in primary productivity at Ocean Station P (50°N, 145°W) in the subarctic Northeast Pacific Ocean. *Can. Spec. Publ. Fish. Aquat.*, **121**, 107–117.

Wroblewski, J. S. (1977): A model of phytoplankton plume formation during Oregon upwelling. *J. Mar. Res.*, **35**, 357–394.

Chapter 3

Characteristics of spatial distributions of biological variables in the three-dimensional model

3.1 Introduction

How the pelagic ecosystem in the ocean responds to changes in its environments is an urgent problem awaiting an answer. The response may lead to variation in the strength of the biological pump, and thereby it may have an impact on the climate. However, due to the insufficiency of reliable data on the variation of the biological pump, and for the sake of simplicity, the present ocean models for predicting the future CO_2 change (*e.g.*, Sarmiento and Orr, 1992) have assumed that there has been no variation in the biological pump over the whole ocean. This assumption is partly supported by Falkowski and Wilson (1992) who showed that chlorophyll concentration inferred from Secchi disk data collected in the North Pacific do not suggest any significant change over the past 70 years. There are, however, some indications that the ocean biota is indeed experiencing changes on the decadal time scale: Venrick *et al.* (1987) suggested that in the subtropical gyre of the North Pacific, chlorophyll concentration may have been doubled since 1968; Brodeur and Ware (1992) reported that in the northeastern Pacific doubling took place in zooplankton biomass between the periods 1956 - 1962 and 1980 - 1989; Roemmich and McGowan (1995) stated that zooplankton biomass has decreased by 80 percent off southern California. In addition, decadal changes on the higher trophic level (*e.g.*, Beamish and Bouillon, 1993) may be reflecting some changes on the lower trophic level, which may alter the strength of the biological pump.

It is recognized that, in many cases, the causes of ecosystem changes can be attributed to those in physical environments. One of the most important physical factors that may affect the oceanic ecosystem is vertical mixing; it may enhance phytoplankton growth by bringing nutrients up to the surface layer from under the euphotic zone where they are abundant, or it may suppress photosynthesis by carrying phytoplankton away from the surface layer where light is replete; whether strengthening of the vertical mixing acts positively or negatively to the oceanic biota depends on a delicate balance amongst various conditions as stated in Chapter 1. Indeed, many authors reporting the ecosystem changes have argued the relation between the ecosystem changes and changes in the mixed layer depth (MLD); for example, Venrick *et al.* (1987) speculated that associated with the decadal climate variation in the North Pacific (*e.g.*, Nitta and Yamada, 1989) the mixed layer deepened and that the biological activities in the subtropical Pacific were enhanced. Furthermore, Polovina *et al.* (1995) showed that winter MLD is changing on the decadal scale over the North Pacific and suggested that there is a possibility that biological activities are deeply affected.

A numerical model can be a powerful tool for investigating the role of the oceanic biota in the biogeochemical cycle and the impact of the variation of the biological pump on the climate. To work on this problem, processes occurring within the mixed layer should be faithfully represented in the model in both physical and biological aspects. The model of Bacastow and Maier-Reimer (1990) is not very suitable for this kind of problem; because their main interest is in reproducing the distribution of tracers in the deep layer, the ecosystem in the surface layer incorporated in their ocean general circulation model (OGCM) is terribly simplified so that the relation between the MLD and the biological activities is only poorly resolved. Improvements were made with their model or other approaches were taken in the subsequent studies (*e.g.*, Bacastow and Maier-Reimer, 1991; Najjar *et al.*, 1992; Anderson and Sarmiento, 1995; Yamanaka and Tajika, 1996; Fasham *et al.*, 1993; Sarmiento *et al.*, 1993), but many of them are for a better reproduction of tracer distribution in the deep layer, not for a more elaborated representation of the pelagic ecosystem. Among them, however, the approach taken by Fasham *et al.* (1993) and Sarmiento *et al.* (1993) is essentially different from the others; they incorporated ecosystem components such as phytoplankton and zooplankton as explicit model variables in an OGCM so that they are directly subject to the vertical mixing. This means that the relation between the mixed layer and the ecosystem is far better represented than in the other models. They applied

their model to the North Atlantic and obtained fairly good results. Although there are many points that should be improved, their model demonstrated potential to deal with the issue of the ecosystem variation.

In this chapter, the ecosystem model which explicitly includes ecosystem components is embedded in an OGCM. The combined model is applied to the North Pacific, where many researchers have reported ecosystem variations. The ecosystem model is the one calibrated in Chapter 2 using its one-dimensional version. It was shown in Chapter 2 that the one-dimensional model bears fairly good results even if it is applied to the totally different oceanic regimes. As a subsequent necessary step of developing the model, the distributions of ecosystem variables are compared with observations. Mechanisms determining distributions in the model are also investigated, especially on the distribution of primary production. This kind of investigation will be able to provide basis for studying the corresponding observed distributions through discussion on the possibility that those mechanisms are functioning also in the real world.

In Section 3.2, model descriptions are given and the results of the OGCM are compared with observation to confirm that the physical model offers realistic environments for the ecosystem model. In Section 3.3, we compare the results of the combined model with observations on the annual mean basis. Comparisons on seasonal variation are made in the next chapter. In Section 3.4, mechanisms determining the spatial patterns in the model are discussed with the focus on primary production, which is the starting point for all of the biological activities in the ocean. Lastly, summary and conclusion of this chapter are provided in Section 3.5.

3.2 Model Description

Here description of the OGCM and the ecosystem model is provided. The OGCM is the one developed at the Center for Climate System Research with some modifications. The ecosystem model is basically the same one adopted in Chapter 2. Thus it is only briefly described focusing on the modifications.

3.2.1 Description of the OGCM

The OGCM employs the primitive equations with hydrostatic, Boussinesq, and rigid-lid approximations. Convective adjustment is achieved by setting the vertical diffusion coef-

Table 3.1. Diffusivity and viscosity in the OGCM. The unit is in cm^2/sec.

Isopycnal diffusivity	1×10^7
Horizontal diffusivity	3×10^6
Horizontal viscosity	8×10^8
Vertical diffusivity	0.3
Vertical viscosity	1.0

ficient to 1000 cm^2/sec when a water column is statically unstable. For the mixed layer model, the Mellor-Yamada's level 2.5 closure scheme (Mellor and Yamada, 1982) which was improved by Kantha and Clayson (1994) is used. Isopycnal diffusion is introduced adopting the method proposed by Redi (1982) and simplified by Cox (1987). The background diffusivity and viscosity are given in Table 3.1 together with the isopycnal diffusivity.

The model domain extends from 122°E to 72°W and from 23°S to 63°N corresponding to the North Pacific. A realistic bathymetry is incorporated within the present resolution described below. The horizontal grid interval is $2° \times 2°$. There are 45 levels in the vertical, and the grid spacing is displayed in Table 3.2. From the sea surface to the intermediate depths, the grid intervals are very small compared to those adopted in other modeling studies. This fine resolution enables the model to reproduce well the stratification in the surface layer and thus the seasonal variation of the mixed layer, which has a significant impact on the ecosystem model as was shown in Chapter 2.

At the sea surface, monthly mean wind stress of Hellerman and Rosenstein (1983) is imposed as the boundary condition; for temperature and salinity, surface values are restored to the monthly mean data of Levitus and Boyer (1994). The damping time is 0.2 days. This value is extremely small even if the thinness of the top level is taken into consideration. The value corresponds to about 1.5 days when the top level has a thickness of 25 m. The typical value in OGCMs is about 30 days for the top layer of 25 m. This value is introduced to prevent the development of MLD from having a large time lag; the value, 30 days, causes a delay of more than one month in seasonal variation of MLD at places where the winter MLD is relatively deep; this delay should be avoided in this study where the time variation of MLD is of great significance. As for time interpolation of these sea surface data, the method of Killworth (1996) is used so that the values imposed on the model equal to those of the original monthly datasets when averaged over a month. As will be explained later, all

Table 3.2. Vertical grid spacing

Grid number	Grid interval (m)	Depth of grid point (m)
1	3	3
2	7	10
$3 \sim 21$	10	200
22	20	220
23	30	250
$24 \sim 32$	50	700
$33 \sim 35$	80	940
36	110	1050
37	150	1200
38	200	1400
39	300	1700
$40 \sim 42$	500	3200
$43 \sim 45$	600	5000

model integrations are made with seasonal variations; the amplitudes are, however, made smaller over the three meridional grids with approaching the southern boundary so that they become zero at the southernmost grids.

At the southern boundary, temperature and salinity are restored to the annual mean values of Levitus and Boyer (1994). The damping time is 50 days at the southernmost grids.

3.2.2 Description of the ecosystem model

The governing equations of the ecosystem model are the same as in Chapter 2 except that the diffusion and advection terms include the horizontal contribution. To express the distribution of sinking flux of particulate organic nitrogen (PON), the formula of Martin *et al.* (1987) is adopted. That is, sinking flux of PON below the depth of 100m is described as follows:

$$F(z) = F_{100}\left(\frac{z}{100}\right)^{-0.858}, \tag{3.1}$$

where F denotes sinking flux of PON, z depth, and F_{100} sinking flux of PON across 100m depth. Above that depth, it is assumed that PON sinks with a constant velocity, 20.0 m/day. This value corresponds to that adoted for the simulation of OWS Papa in Chapter 2, and is larger than that for the BATS site. This larger value is necessary to reproduce

a realistic nitrate distribution; preliminary experiments showed that, if the value is set to the one corresponding to that for the BATS site, the high nitrate concentration in the equatorial region spreads out to the subtropical region due to the Ekman transport and the nitrate distribution becomes totally unrealistic.

The large sinking velocity may act to reduce nutrients from the ocean surface in the oligotrophic region too rapidly. Considering the fact that the subsurface chlorophyll maximum (SCM) is formed at the depth where the light and nutrient condition balance (as will be discussed in Chapter 4), this large sinking velocity can cause deepening of the SCM in the oligotrophic region. Looking at the chlorophyll profiles obtained by the model in the oligotrophic region, however, the SCM is not extremely deep (*cf.*, Fig. 4.19 and Fig. 4.21). The harmful effect seems not to be very serious.

The half saturation constant for nitrate (K_{NO3}) is set to 0.03 μmol/l which is the same value adopted in the simulation at the BATS site, *i.e.*, the oligotrophic region. This choice is justified because the sensitivity to changes in K_{NO3} is far higher in the oligotrophic region than in the eutrophic region; we can easily understand this from the fact that nitrate concentrations in the eutrophic region often have much higher values than those of K_{NO3} while in the oligotrophic region they have similar or smaller values compared with those of K_{NO3}; in many cases, the Michaelis-Menten formula is well saturated in the eutrophic region, and thus making K_{NO3} smaller does not affect the uptake of nitrate.

Although the small K_{NO3} will not do any harm in most of the eutrophic region, it may have some significant effect in fronts of nitrate concentration between the eutrophic and the oligotrophic region or in the mesotrophic region of the central equatorial region because the nitrate concentrations in these regions are comparable to the observed K_{NO3} values. However, it is difficult to incorporate the spatial variation of K_{NO3}. One way to include it in the model is to make K_{NO3} be a function of ambient nitrate concentration so that K_{NO3} becomes large when the concentration is high and *vice versa*, following the suggestion of Harrison *et al.* (1996) that the value of K_{NO3} shows an excellent positive correlation with the ambient nitrate concentration. A preliminary experiment showed, however, it was difficult to prevent the equatorial high nitrate concentration from penetrating into the oligotrophic region if the K_{NO3} variation is incorporated as in the way described above. It is not very diffucult to understand the reason; when the nitrate concentration rises in the frontal region between the equatorial eutrophic region and the subtropical oligotrophic region, the K_{NO3} value also rises and the uptake rate of nitrate decreases; thus, the equatorial high

nutrient concentration easily penetrate into the subtropical region. The incorporation of K_{NO3} variation introduces an undesired positive feedback mechanism. We concluded that it is better to let K_{NO3} be constant for the present.

The choice of the value of the half saturation constant for ammonium (K_{NH4}) is not very straightforward because ammonium concentration is similar to values of K_{NH4} even in the eutrophic region. Here, considering the relative importance of regions with high productivities, it is set to 1.0 μmol/l, which is the value adopted in the simulation in the eutrophic region, OWS Papa.

Furthermore, the decay rate of DON is changed rather drastically from the value in Chapter 2 to 0.01 day^{-1}. This change corresponds to taking the role of semi-refractory DON into consideration (Kirchamn *et al.*, 1993), in contrast to the experiments in Chapter 2 where it is neglected. This is incorporated in order to prevent the region with high nutrient concentration from spreading out to the subtropical region so that an "oligotrophic region" vanishes from the North Pacific. Preliminary experiments showed that this parameter change affects only on the nutrient concentration near the equator; it had only minor effects on the dynamics of the model in other regions. Together with the incorporation of the production of DON, the photosynthetic rate V_{max} is increased to 1.2 day^{-1} from the value in Table 2.1 of Chapter 2 (1.0 day^{-1}), and the ratio of extracellular excretion to photosynthesis is also increased to 0.3 from 0.135.

Nitrate concentrations near the southern boundary are restored to the values of Levitus *et al.* (1993) in the same way as for temperature and salinity.

3.2.3 Time integration

We take two steps to spin up the OGCM. First, we integrate it using the acceleration method of Bryan (1984) for 2000 deep water years (DWYs) with time step of six hours. This integration period corresponds to 200 years for the depths above 1000 m. For this step, the vertical diffusivity and viscosity above 50 m depth are set to a large constant value, 10 cm^2/sec without the closure model. Next, the mixed layer model is incorporated, and the OGCM is integrated for 50 years without the acceleration method. The time step is one hour. In the year 50, the upper layer above several hundred meters almost reaches a steady cycle, and it shows only negligible trends. Then, the ecosystem model is integrated together with the OGCM taking the results in the year 50 as the initial conditions for the physical fields. The time step is two hours for the ecosystem model and one hour for the

OGCM. The averaged values of the variables in the OGCM over the two time steps are provided to the ecosystem model. The initial values for nitrate are taken from Levitus *et al.* (1993). For other biological variables except phytoplankton and zooplankton, the initial values are set to zero everywhere. The initial values for phytoplankton are 0.053 μmolN/l (corresponding to a chlorophyll concentration of 0.1 μg/l using the ratios adopted in Section 2.3.3) above 100m depth and zero below that depth; for zooplankton, 0.12 μmolN/l above 100m and zero below. The integration period is six years. There still exists a trend in nitrate concentration but a steady cycle is established for other variables in the ecosystem model (Fig. 3.1). Although the nitrate trend is a subject we have to work on in the future, we decide to proceed to analysis of the chlorophyll seasonal variation, which have already established a steady cycle.

Monthly averaged data are created in the model. Results in the sixth year, comprised of the twelve datasets for each variable, will be analyzed.

3.2.4 Comparison of results of the OGCM with observations

Before comparing the results of the ecosystem model with observation, it will be helpful to see to what extent the OGCM offers realistic environments to the ecosystem model.

Fig. 3.2 shows temperature and salinity structures from the sea surface down to the depth of 1000 m along 180°. The modeled temperature structure bears overall resemblance with the observation but shows the feature that waters at intermediate depths are too warm compared with the observation, which is common to all modeling efforts (*e.g.*, Hirst and Cai, 1994). The model yields salinity minima at intermediate depths though the strength is weaker than the corresponding minima in the observation. The modeled salinity minimum whose center is around 23°N and 600 m depth seems to be isolated but is actually connected to the low salinity water to the east of it.

Next we look at the circulation near the surface. Fig. 3.3 shows the annual mean current averaged over the upper 100m. Main features of the surface current are basically reproduced; the Kuroshio and the Oyashio flow along the western boundary of the domain, the strongly divergent flow is found along the equator, and the Alaskan gyre is seen in the northeastern part of the domain. A closer look can, of cource, reveal some defects of the current field; the separation point of the Kuroshio is located further north than that of observation (*e.g.*, Wyrtki, 1975); the complicated flow along the northern side of the equator is only partly reproduced by the model. (for example, the Equatorial Counter Current does

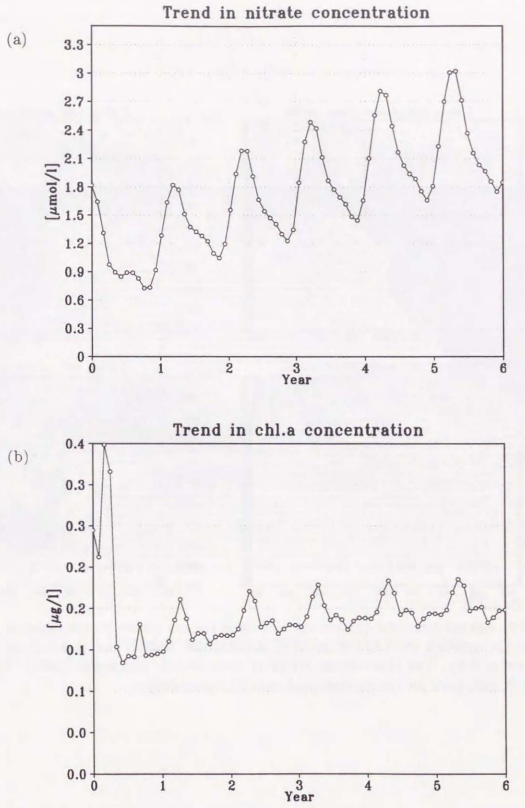

Fig. 3.1. Time variation of (a) nitrate and (b) chlorophyll in the uppermost layer averaged over the whole domain.

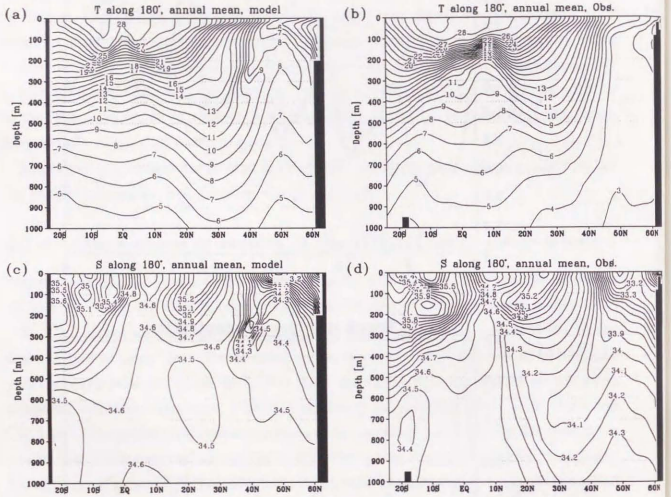

Fig. 3.2. Annual mean structure along 180° from the sea surface to the depth of 1000 m for (a) the modeled and (b) the observed temperature, and (c) the modeled and (d) the observed salinity. The observations are taken from Levitus and Boyer (1994). The units are in °C and p.s.u for temperature and salinity, respectively.

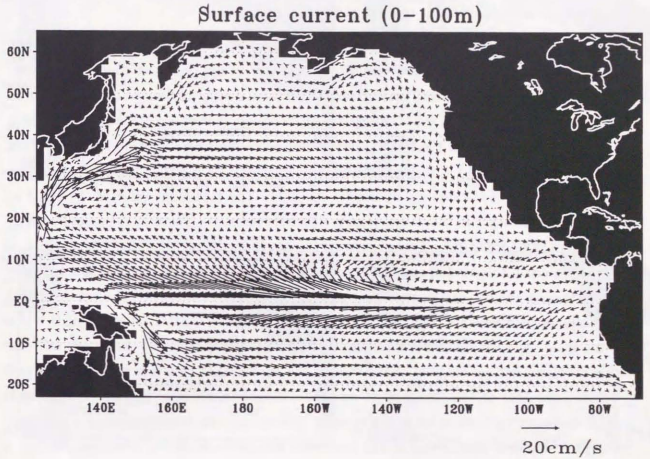

Fig. 3.3. Annual mean current averaged over the upper 100m.

not exist in the western part of the equatorial region.) These defects are inevitable in this kind of model with such a coarse resolution. In practice, however, the horizontal flow does not directly affect the growth of the phytoplankton, *i.e.*, the contribution from horizontal advection in the governing equation of phytoplankton (Eq. 2.21) is small compared with other terms such as photosynthesis and grazing. It indirectly affects the phytoplankton growth mainly through its impact on the MLD distribution and by generating vertical flow though its divergence and convergence. Thus, how well the model reproduces the MLD distribution and the intensity of vertical flow is dicussed next.

MLD needs to be realistically reproduced for the purpose of this study, *i.e.*, modeling of the oceanic ecosystem. Here, the MLD is defined as the depth at which the density difference from the sea surface first exceeds the critical density difference corresponding to a temperature difference of 0.5 °C at each point. The distributions of MLD are displayed in Fig. 3.4 for March, when the mixed layer is deepest at most locations, and August, when it is shallowest. In March, the model well reproduces the feature that the MLD is deep in the eastern part of the domain at middle latitudes. The maximum value of the MLD is, however, much larger in the model than in the observation ($\sim$ 500 m in the model while $\sim$ 200 m in the observation). This discrepancy arises from the problem of the separation of the Kuroshio; in this kind of coarse resolution model, the Kuroshio penetrates much further north than in reality, carrying warm water up to the north: the water is then cooled by the imposed temperature originating from the real Oyashio, thus causing the MLD which is too deep. Adopting a longer damping time for the surface boundary condition will ease this problem, but we consider that avoiding the lag in MLD variation is more important because the goal of this thesis is to analyze seasonal variations. Besides, the modeled MLD is deeper on both sides of the equator. The reason for this discrepancy is not clear but presumably it is also due to the coarse horizontal resolution; it is recognized that a much finer meridional resolution ($\sim 0.3°$) is necessary to realistically reproduce the thermal structure near the equator (*e.g.*, Rosati and Miyakoda, 1988). In August, the decreasing tendency of MLD toward the north is well reproduced in the model. The unrealistically deep mixed layer near the equator, however, still remains.

Vertical velocity near the sea surface is also important for the ecosystem model because it contributes to the vertical transport of nutrients. At mid- and high- latitudes, it is determined by the Ekman velocity, and is not strongly dependent on the model. In the equatorial region, however, it is determined through rather a complicated process and is

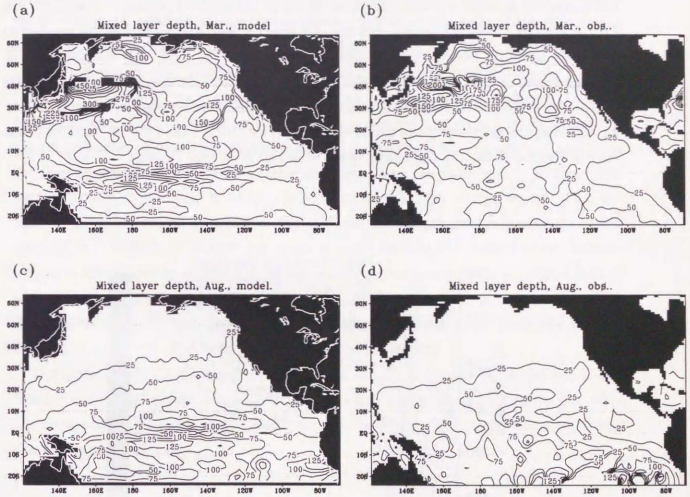

Fig. 3.4. Mixed layer depth (MLD) for March in (a) the model and (b) the observation, and for August in (c) the model and (d) the observation. See text for the definition of MLD. The MLD in the observation is derived from the data of Levitus and Boyer (1994). The units are in meter.

model dependent. It will be needed to check the vertical velocity in the model. Fig. 3.5 depicts its distribution along the equator. Upwelling dominates almost all through the region and it takes the maximum value of $\sim$ 350 cm/day around 150°W at the depth of 60 m. Halpern *et al.* (1989) calculated the equatorial upwelling between 140°W and 110°W on the basis of mooring current meter data from 1983 to 1984; they reported that it takes the maximum value of $\sim$ 250 cm/day near 140°W at the depth of 50 m, and that there is a decreasing trend toward the east. Bryden and Brady (1989) also estimated the equatorial upwelling based on mooring current meter data from 1979 to 1981; they showed that the average profile of upwelling between 152°W and 110°W takes the maximum value of $\sim$ 400 cm/day at the depth of 70 m. Comparing the model result with these observations, it can be said that the intensity of the model upwelling is well within the range of data, and that its distribution shows the decreasing trend from 150°W toward the east.

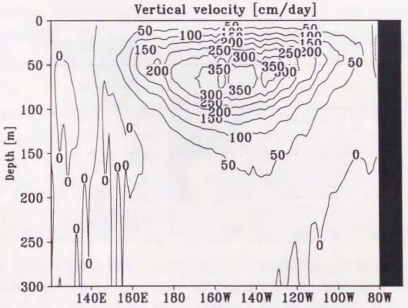

Fig. 3.5. Annual mean vertical velocity along the equator. The unit is in cm/day. Positive values indicate upwelling.

3.3 Comparison of results of the ecosystem model with observations

3.3.1 Nitrate

Although the integration period of the ecosystem model (six years) is not long enough to modify the initial condition of nitrate over the whole domain including the deep ocean, it is sufficient to affect the nitrate distribution at depths above $\sim$ 200 m. Comparison of the nitrate distribution with observation serves as a test of the model performance.

Fig. 3.6 plots annual mean nitrate concentrations averaged over the surface 100 m. The model maintains the overall pattern that nitrate is more abundant in the equatorial and the subpolar region, where the Ekman upwelling transports nitrate upward. It also keeps the high concentration due to the coastal upwelling along California coast. In the north-eastern part of the domain, however, the concentration is lower in the model. That the modeled MLD is too shallow in March (Fig. 3.4) seems to be a reason for the disagreement, although it is difficult to identify the ultimate cause because the surface nitrate concentration is determined by combination of various factors such as upwelling, vertical mixing, and sinking of PON. In the eastern part of the domain, nitrate is too scarce at $\sim$ 10°N. This is presumably because the upwelling induced by wind stress curl along this latitude is only poorly resolved due to the coarse horizontal resolution.

As shown in Fig. 3.1, the nitrate concentration has not yet reached a steady state. The tongue of the high concentration along the equator is still gradually spreading out while the nitrate in the subpolar gyre is also gradually increasing. The magnitude of the trend can be grasped in Fig. 3.7.

3.3.2 Chlorophyll

Comparison with satellite data

In Fig. 3.8, the modeled chlorophyll abundance near the sea surface is compared with the satellite observation by Coastal Zone Color Scanner (CZCS) during 1978 - 1986. In this figure, nitrogen based phytoplankton abundance is converted to chlorophyll concentration using the same ratio as in Section 2.3.3. The model data are averaged over the surface 10 m so that they can be directly compared with CZCS data, which can provide averaged information only for the surface layer of about 10 m (*e.g.*, Gordon *et al.*, 1982).

(a)

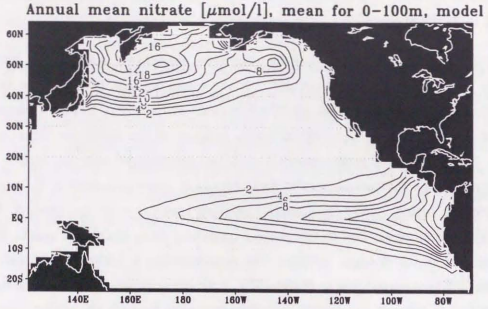

(b)

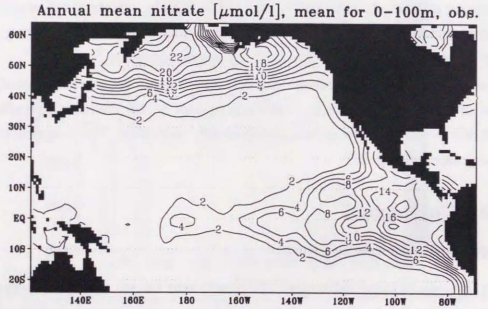

Fig. 3.6. Annual mean nitrate concentration averaged over the surface 100 m for (a) the model and (b) the observation (Levitus *et al.*, 1993). The unit is in μmol/l.

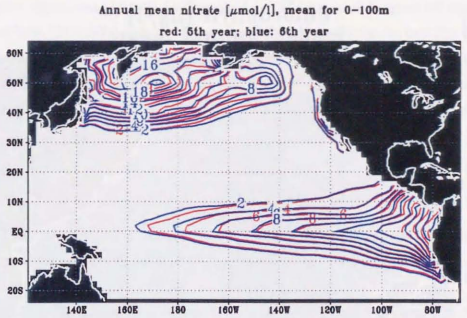

Fig. 3.7. Annual mean nitrate concentration averaged over the surface 100 m for the fifth year (red contourlines) and the sixth year (blue contourlines). The unit is in μmol/l

The model bears the overall tendency that the concentration is high in the subpolar and the equatorial region, and low in the subtropical region corresponding to the nitrate distribution. Also, the high concentration induced by the California upwelling is reproduced in the model.

There are, of course, disagreements between the model and the observation; the model concentration is too high in the equatorial and the subtropical region, and too low in the subpolar region; near the equator, the highest abundance occurs on both sides of the equator along about 5° latitudes, unlike in the observation where it occurs along the equator.

The problem of lower chlorophyll in the subpolar region is partly due to the error in the satellite measurement, as well as inadequacy of the model; CZCS tends to overestimate chlorophyll abundance at latitudes higher than $\sim$ 40°N especially in fall (Yoder *et al.*, 1993). According to Anderson *et al.* (1977) who summarized surface chlorophyll data at Ocean Weather Station (OWS) Papa (50°N, 145°W) during 1959 - 1976, the annual mean surface concentration is about 0.3 μg/l while it is about 0.6 μg/l in the CZCS observation at this location.

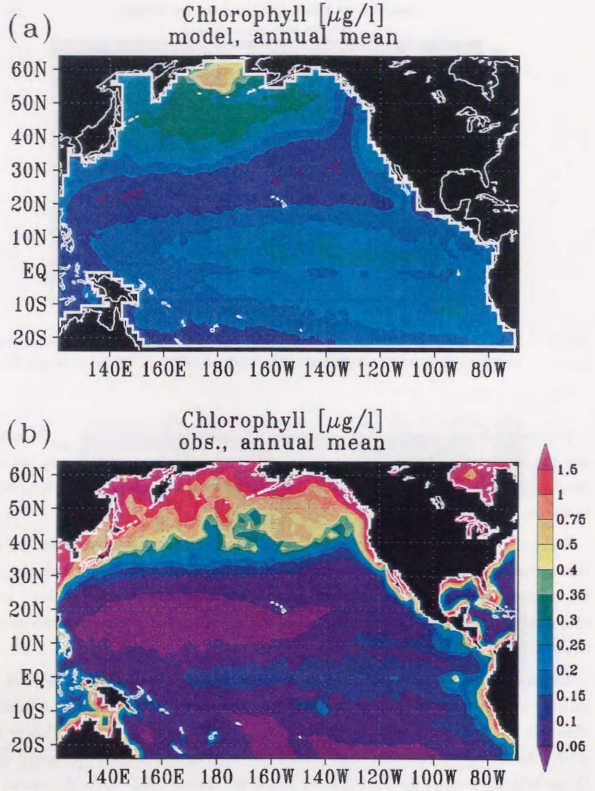

Fig. 3.8. Annual mean chlorophyll concentration obtained by (a) the model and (b) the satellite observation. The model data are averaged over the uppermost 10 m. The unit is in μg/l. The observation shows the mean for the observation period 1978 - 1986.

The higher concentrations in the subtropical and the equatorial region are brought about perhaps because the model does not incorporate the photoadaptation process; as discussed in Section 2.4.3, the N/Chlorophyll ratio of phytoplankton tends to increases near the sea surface in the subtropical and the equatorial region to adapt to the intense light. The low chlorophyll concentration in the observation does not necessarily reflect correspondingly low phytoplankton biomass.

The chlorophyll maxima on both sides of the equator are caused by the vertical mixing there, which is too strong as is evidenced by Fig. 3.4. Near the equator, chlorophyll is more abundant at the depth of about 60 m. Beside the equator, however, the chlorophyll maximum at that depth is destroyed by the strong vertical mixing so that the high concentration appears at the sea surface. If the chlorophyll is integrated over the upper 100 m, the maximum exists exactly along the equator (*cf.* Fig. 4.2).

As a whole, it can be said that the model result is reasonably well compared with the observation: the obtained values are within the order of the observation; it can reproduce the overall pattern that chlorophyll is abundant in the subpolar and the equatorial region and scarce in the subtropcal region. The same level of agreement as in the physical model can not be expected in the ecosystem model; there is no undoubted governing equations in ecosystem modeling unlike in physical modeling.

Comparison with in situ data

Chlorophyll data along 175°W has been extensively observed by the Northwest Pacific Carbon Cycle Study (NOPACCS, Ishizaka and Ishikawa, 1991). The data in 1992 (NOPACCS, 1992) are displayed in Fig. 3.9 with the corresponding model result.

The model captures some of the features in the observation: The depths of the subsurface chlorophyll maximum (SCM) in the model agree well with those in the observation; the SCM in the model deepens in the subtropical gyre as in the observation; an isolated maximum at the equator exists in both the model and the observation. Moreover, the absolute values of the model concentration are well compared with those in the observation. The extremely large value at 40°N is not a permanent feature as it is not found in the observation of another year (Ishizaka *et al.*, 1994). On the other hand, the isolated maximum at the equator seems to be persistent except during the period of *El Niño* (Bidigare and Ondrusek, 1996). Besides, the cause for the higher concentration near the sea surface obtained by the model is presumably the photoadaptation as is explained above and also

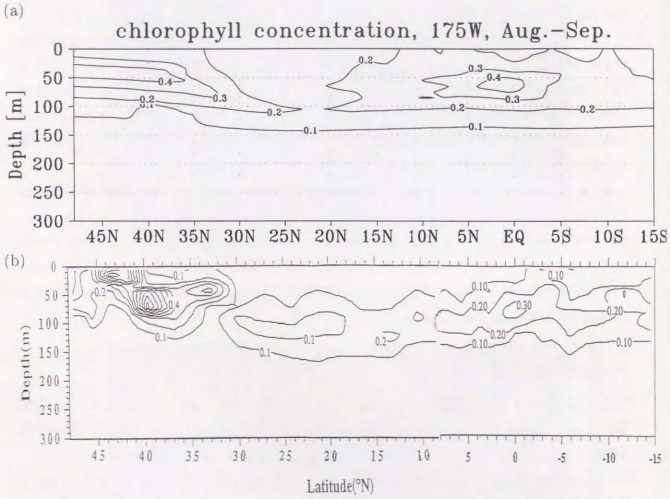

Fig. 3.8. Chlorophyll concentration along 175°W obtained by (a) the model and (b) the observation conducted as a part of the Northwest Pacific Carbon Cycle Study (NOPACCS) from August 7 to October 5 in 1992. Correspondingly, the model result is a mean for August through September.

in Section 2.4.3.

Chavez and Smith (1995) collected chlorophyll data in the eastern Pacific and provided the distribution of integrated chlorophyll abundance. Fig. 3.10 shows the data and the corresponding model result. It lies within the range of the data scattering and reproduces the trend that the concentration is high in the equatorial and the subpolar region and low in the subtropical region. Interestingly, the overestimation by the model is not as large as it looks in Fig. 3.8.

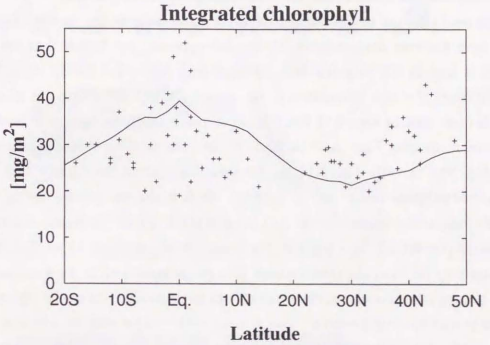

Fig. 3.10. Latitudinal distribution of depth-integrated (0 - 200 m) chlorophyll obtained by the model (annual mean, solid line) and observations (Chavez and Smith, 1995, crosses). The data are collected within a longitudinal range of 160°W - 100°W in various seasons. The observation points are shown in Chavez *et al.* (1995). The model result is also averaged over the longitudinal range.

The model shows better similarity with the observations in Figs. 3.9 and 3.10 than in Fig. 3.8. Considering that the integrated phytoplankton biomass is more important for the geochemical cycling than that in the shallow surface layer, the extent of the agreement is satisfactory.

3.3.3 Zooplankton

Bogorov *et al.* (1968) and Reid (1962) summarized data on zooplankton biomass from many literatures as shown in Figs. 3.11 (b) and (c). The unit of the original data of Bogorov *et al.* (1968) (mg wet weight per m^3) has been converted into μmol Nitrogen per liter (μmolN/l) by Glover *et al.* (1994) so that a direct comparison can be made with the model result (Fig. 3.11 (a)). The model zooplankton biomass is averaged over the surface 150 m, below which no significant biomass is found at any point of the domain. Although a conversion factor between the unit in Figs. 3.11 (a) and (c) has not been firmly established, qualitative dicussion is possible and the conversion is not forcibly made.

It can be seen that the model biomass is of the same order as that in Fig. 3.11 (b). In addition, as in the case of chlorophyll, the model represents the feature that the biomass abundance is high in the subpolar and the equatorial region and low in the subtropical region. Although the high abundance in the model along $\sim 42°$N does not exist in Fig. 3.11 (b), it does exist in Fig. 3.11 (c). The abundance along the equator is much higher in the model comparing Figs. 3.11 (a) and (b), but the problem seems less serious if we compare Fig. 3.11 (a) with Fig. 3.11 (c); the abundance along the equator is of the same order as in the subpolar region in Fig. 3.11 (c), which is also the case for the model.

From the comparison between Figs. 3.11 (b) and (c), it can be recognized that the observations themselves are not very reliable. We should be satisfied here to see that the model result is not very far from the observations. The rough agreement in the zooplankton distribution between the model and the observations suggests that the model phytoplankton is under a proper grazing pressure. The grazing is the major sink for the model phytoplankton and thus it is very important for the phytoplankton seasonal variation, which will be analyzed extensively in the next chapter.

3.3.4 Net primary production

Fig. 3.12 (a) shows the annual net primary production (NPP) obtained by the model. In the model, net primary production is defined as the phytoplankton growth term (DON* formation is excluded) minus the "respiration" term, both of which are described in Section 2.2. For the conversion from nitrogen based values to carbon based ones, the same ratio as in Section 2.3.3 is used. As for observational estimation of NPP, global maps of NPP

*Dissolved Organic Nitrogen

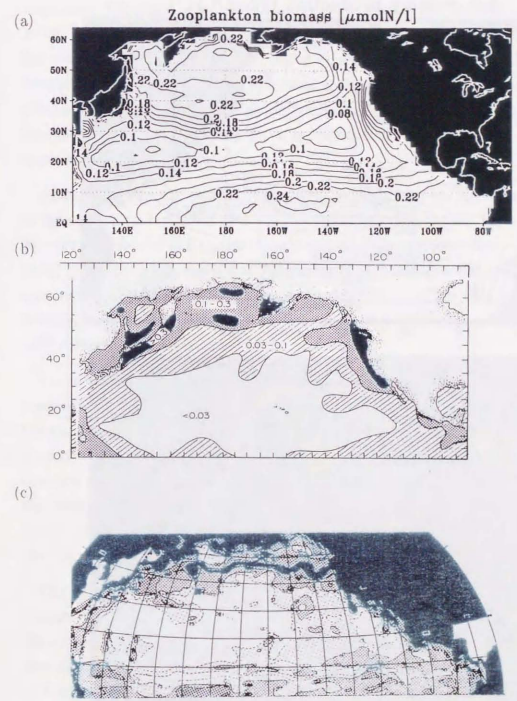

Fig. 3.10. Distribution of zooplankton biomass based on (a) the model and the data compiled by (b) Bogorov *et al.* (1968) and (c) Reid (1962). The model result is the averaged over the surface 150 m. The units are in μmolN/l for (a) and (b) and in ml/(10^3m^3) for (c). Darkest shading in (c) indicates values approaching 1 ml/m^3.

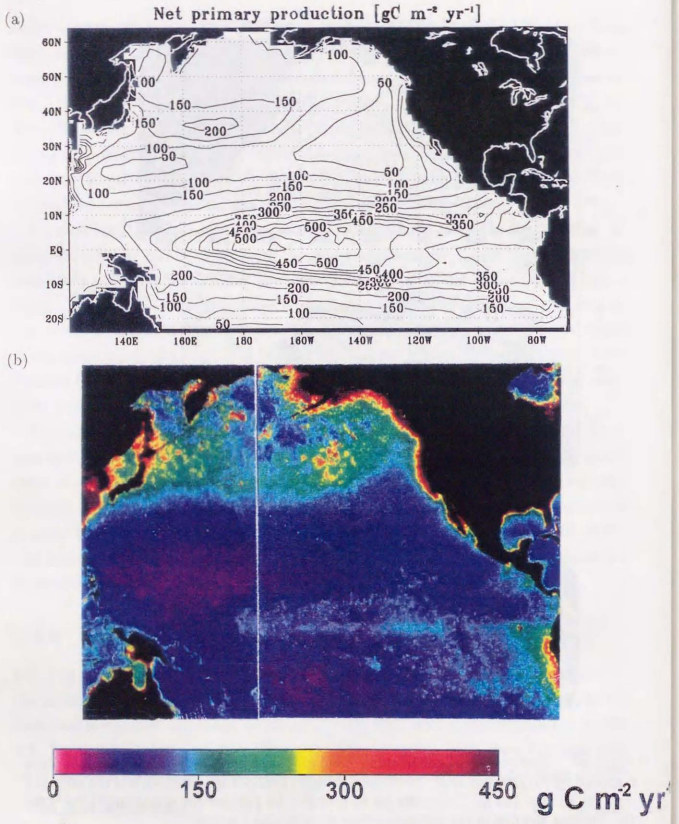

Fig. 3.11. Net primary production (a) obtained by the model and (b) derived from the satellite observation and empirical laws (redrawn from Behrenfeld and Flakowski, 1997). The unit is in g carbon per m^2 per year (gC m^{-2} yr^{-1}).

derived from the CZCS measurement plus empirical laws have been proposed by some researchers (Longhurst *et al.*, 1995; Antoine and Morel, 1996; Behrenfeld and Flakowski, 1997). Although some minor differences can be found among the three maps cited above, the overall patterns and the approximate values are similar to one another. A detailed comparison among the three maps is made in Behrenfeld and Flakowski (1997). Here we compare the model result with the map of Behrenfeld and Flakowski (1997) because it is the latest (this map will be referred to as "observation" though strictly speaking it is not based on the pure observation).

Again, the values are generally high in the subpolar and the equatorial region and low in the subtropical region for both the model and the observation. The zone of high NPP between the subpolar and the subtropical region seen in the observation seems to be reproduced by the model though it does not extend to the eastern boundary in the model. This maximum zone is particularly interesting because chlorophyll is more abundant at higher latitudes for both the model and the observation (Fig. 3.8). The mechanism forming this NPP distribution is investigated in the next section.

The major discrepancy occurs in the equatorial region. The maximum value in the model exceeds 500 gC m^{-2} yr^{-1} while in the observation it is only $\sim$ 150 gC m^{-2} yr^{-1}. One of the reason for this overestimation is probably the simple extrapolation of the temperature dependence of photosynthetic rate; although the dependence is based on Eppley (1972), his equation (incorporated in Eq. (2.1)) seems to become unreliable around $\gtrsim$27°C because the number of experimental data is small in this temperature range. In the model, the annual mean temperature above 100 m is *ca.* 28°C where the NPP is much higher than the observation.

The uncertainty of NPP estimation in the equatorial region is, however, quite large because of the high variability there. Chavez *et al.* (1996) reported that the mean NPP for the equatorial Pacific from 90°W to 180°, 5°S to 5°N is 330 gC m^{-2} yr^{-1}, a far larger value than that seen in Fig. 3.12 (b). The corresponding average of the model NPP is 450 gC m^{-2} yr^{-1}. Therefore, the NPP in the model may not be as unrealistic as it looks in Fig. 3.12 though it is still higher than in the observation.

The photosynthesis is the major source for the phytoplankton. Thus, together with the result shown in Section 3.3.3, it turns out that both the source and the sink (the grazing) may be considered as having a proper order.

3.4 Discussion on the distribution of the primary production

Here, detailed analysis is conducted on the spatial patterns obtained by the model. The focus is on the NPP because it is the starting point for all of the biological activities in the ocean, and almost the only variable on which basin-scale, depth-integrated data are available. Mechanisms forming the patterns are examined and their applicability to the real ocean is discussed.

3.4.1 Production minima in the subtropical region

In the subtropical region, there are two minima in the eastern and the western part of the gyre (Fig. 3.12 (a)). These areas of low NPP is formed by the Ekman downwelling, whose distribution derived from the data of Hellerman and Rosenstein (1983) is shown in Fig. 3.13 (a). It is seen that the locations of the NPP minima well correspond to those of strong downwelling. The downwelling carries nitrate away out of the euphotic zone to the deeper layer. Low nitrate concentrations in the model can be found corresponding to the strong downwelling (Fig. 3.13 (b)).

In the data of Levitus *et al.* (1993) shown in Fig. 3.13 (c), low nitrate concentrations at around 33°N, 135°W and 25°N, 160°E seem to be reflecting the downwelling maxima though their spreadings are rather narrow. Thus it is possible that in reality the Ekman downwelling is also acting to suppress photosynthesis by reducing nitrate.

In Fig. 3.12 (b), however, the "observed" NPP shows the minimum only in the western part of the subtropical region instead of the double minima found in Fig. 3.12 (a). The "observed" NPP in the eastern part is larger than that in the western part while the Ekman downwelling is more intense in the eastern part. Going into detail on this problem will be beyond the scope of this thesis because the inconsistency is outside the model, that is, between Figs. 3.12 (b) and 3.13 (c). Here, we merely point out this apparent conflict between the distributions of the Ekman velocity and the NPP.

3.4.2 Production maximum along 35°N

In Fig. 3.12 (a), a belt of high NPP is extending to the east from the coast of Japan along $\sim$ 35°N. It seems to have a counterpart in the observation (Fig. 3.12 (b)). Thus it is very intriguing to examine the reason the NPP is large here.

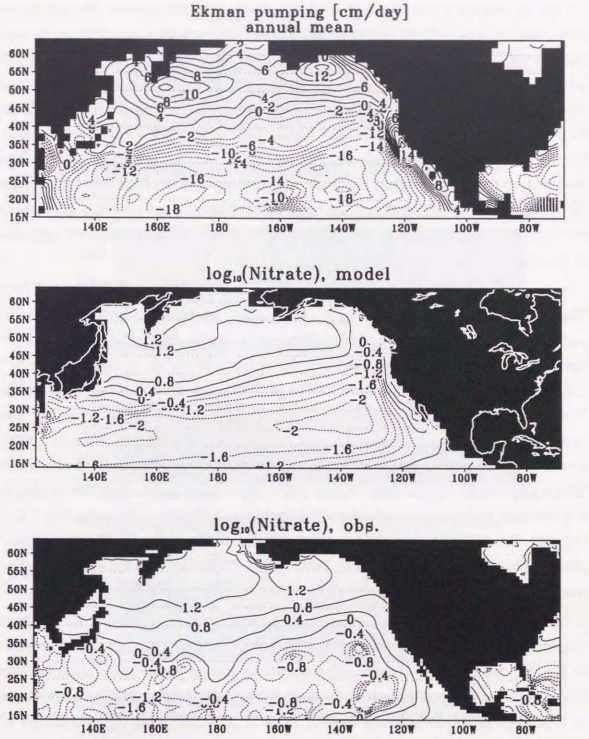

Fig. 3.13. (a) Ekman velocity (cm/day) derived from the data of Hellerman and Rosenstein (1983) and annual mean nitrate concentration averaged over 0 - 100 m in (b) the model and (c) the observation (Levitus *et al.*, 1993). The nitrate concentrations are expressed in logarithm of μmol/l. In (b) and (c), contourlines out of the range from -2 to 1.2 are not drawn.

First, we investigate why the high NPP belt exists along this latitude. In order to understand this, the term for photosynthesis in Eq. (2.1) is decomposed into three parts, namely, dependence on nutrient ($[NO_3/\{NO_3+K_{NO3}\}]\exp\{-\Psi NH_4\}+NH_4/\{NH_4+K_{NH4}\}$), temperature ($\exp\{kT\}$), and light ($\{I/I_{opt}\}\exp\{1-I/I_{opt}\}$). Fig. 3.14 shows them together with their product along 169°E. It is clearly seen that the nutrient condition is favorable for photosynthesis to the north and the temperature condition is so to the south. Besides, the light condition does not have distinct meridional gradient. After all, as can be seen from Fig. 3.14 (d), the overall condition becomes most suitable for photosynthesis at $\sim$ 35°N where both the nutrient and the temperature condition are modestly good. In other words, this is the location where the nutrient and the temperature condition are balanced for photosynthesis.

Next, we examine the mechanism forming the zonal distribution on this high NPP belt. The maximum at $\sim$ 170°E is brought about mainly because nitrate is vigorously transported from under the euphotic zone in summer at this location. To see this, the photosynthetic term is again decomposed and the nutrient condition in August along 34°N is displayed in Fig. 3.15 (a). Around 170°E, the condition is favorable for photosynthesis. The reason for this favorite condition can be found in Fig. 3.15 (b), where the vertical diffusion coefficient is shown; right under the euphotic zone (to the depth of $\sim$ 100 m), a watermass with large diffusivity is lying at $\sim$ 170°E and contributing to enrich nitrate. This watermass is, in turn, formed from winter to early spring when surface cooling forms a watermass with weak stratification and thus large diffusivity. By comparing Fig. 3.15 (b) with Fig. 3.15 (c), where the vertical diffusion coefficient in March is displayed, it is clearly seen that the watermass with large diffusivity in Fig. 3.15 (b) is a remnant of the one with weak stratification in Fig. 3.15 (c).

Concerning the mechanism determining the zonal structure along $\sim$ 35°N, the deep, vigorous vertical mixing from winter to early spring is important. However, as can be seen in Fig. 3.4, the depth to which the intense vertical mixing penetrates is much shallower in the observation than in the model; in March, it is only $\sim$ 150 m in the observation while it is as deep as $\sim$ 300 m in the model. Thus, it is unlikely that this mechanism is also functioning in the real world though the possibility can not be completely denied.

Meridionally, on the other hand, the high NPP belt in the model seems to exist also in the observation (Fig. 3.12 (b)) as mentioned above. For creating Fig. 3.12, Behrenfeld and Flakowski (1997) have adopted an empirical relation between temperature and

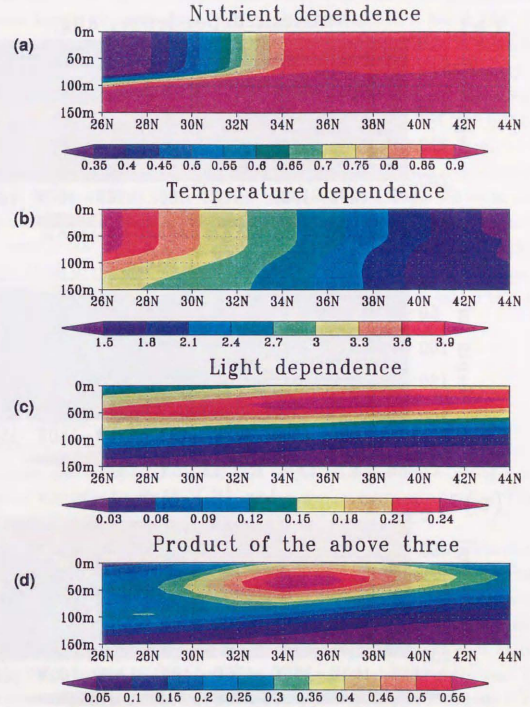

Fig. 3.14. Decomposition of the term for photosynthesis in Eq. (2.1) along 169°E. The upper three figures represent dependence on (a) nutrient, (b) temperature, and (c) light, respectively. The product of the three parts is displayed in (d). The model results are taken from January as an example.

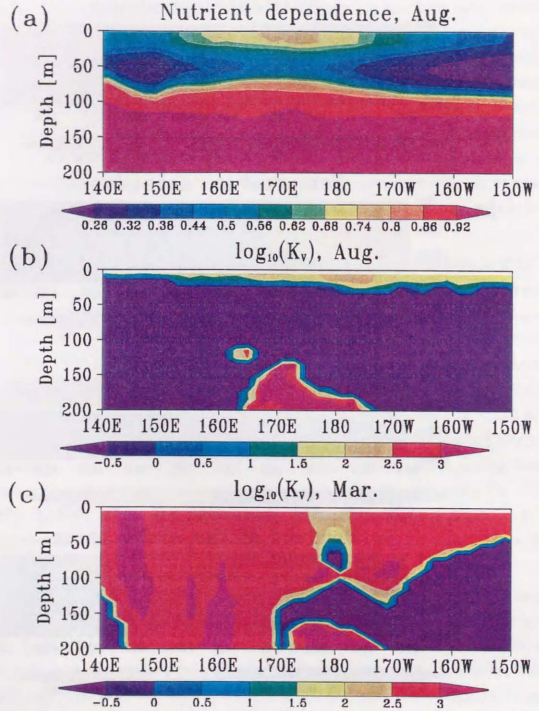

Fig. 3.15. (a) Nutrient condition for photosynthesis based on the decomposition of the term for photosynthesis in Eq. (2.1), and vertical diffusion coefficient expressed in common logarithm for (a) August and (c) March.

photosynthetic rate which is similar to that in our model, that is, the photosynthetic rate increases rapidly with temperature [†] . Therefore, the high NPP belt in Fig. 3.12 (b) may not be independent from that in our model. The empirical relation in Behrenfeld and Flakowski (1997) is, however, based on a compilation of *in situ* data unlike that exploited in our model (Eppley, 1972), which is derived from laboratory experiments. In that sense, the agreement between Figs. 3.12 (a) and (b) on the existence of the high NPP belt provides a certain observational basis for the mechanism forming the belt in the model.

Besides, an area of high NPP is also found in the central equatorial region. The NPP of this area is, however, much higher than that in the observation, thus it will not be examined in detail. Here we will suffice it to say that the same mechanism forming the meridional distribution around 35°N is also in effect; the temperature condition is more suitable for photosynthesis to the west because water temperature is higher in the west than in the east, and the nutrient condition is so to the east as seen in Fig. 3.6; around 180°, the two conditions are best balanced.

3.5 Summary and conclusion

We have developed the three-dimensional ecosystem model embedded in the OGCM. The ecosystem model was calibrated in the previous chapter using its one-dimensional version at a couple of ocean weather stations. The vertical resolution of the OGCM is very fine compared with other OGCMs, from the sea surface to the intermediate depths. The mixed layer model is incorporated in the OGCM.

The OGCM provides the basically realistic environments for the ecosystem model concerning the MLD and the vertical velocity. The overall distribution of the modeled MLD is similar to that in the observation. Intensity of the equatorial upwelling is within the range of data and it shows the decreasing trend from 150°W toward the east like in the observation. The major defects of the model are the MLD off Sanriku coast which is too deep in March and the MLD on both sides of the equator throughout the year. Caution must be taken on these defects when the modeled seasonal variation is analyzed in the next chapter.

The results of the ecosystem model are compared with observations. The model bears

[†] In the relation adopted by Behrenfeld and Flakowski (1997), the increase of the photosynthetic rate ceases at about 20°C. Nevertheless, it is possible that the same mechanism as in our model is working also in their calculation because annual mean SST to the north of 35°N is less than 20°C.

similar distributions of nitrate, chlorophyll, zooplankton, and NPP to those in the observations, in that their values are of the same order as in the observations and that the general trend common to these variables (the values are small in the subtropical region and large in the subpolar and the equatorial region) is reproduced. There are, however, notable discrepancies between the model and the observations. The chlorophyll concentration at the sea surface in the model is higher in the subpolar region and lower in the subtropical and the equatorial region than in the CZCS observation; the former can be ascribed at least partly to the error in the CZCS data, while the latter to the neglect of the photoadaptation process in the model. The NPP in the equatorial region is higher than in the observation; probably this problem arises because the temperature dependence of the photosynthetic rate is simply extrapolated to the equatorial region.

The mechanisms determining the distribution of the modeled NPP are examined. The low NPP in the eastern and the western part of the subtropical region is caused by the wind-induced downwelling. The western low NPP is also seen in the observation, but the eastern one can not be found. The reason for the discrepancy on the eastern NPP is very difficult to identify because the nitrate observation supports the model result in contrast to the NPP observation. On the other hand, the high NPP belt along $\sim 35°$N in the western North Pacific is formed because at this latitude the nutrient and the temperature condition are best balanced for photosynthesis. The high NPP belt is also seen in the observation and it is possible that the mechanism is applicable to the real ocean. The NPP takes the highest value at $\sim 170°$E on this belt because nitrate is vigorously transported by the vertical mixing even in summer at this location. However, it is unlikely that the active nutrient transport is also occurring in the real ocean.

On the whole, the model results are acceptable in the present state of the art in ecosystem modeling on the basin scale. The similarity of the model results to the observations is not worse than that in, for example, Sarmiento *et al.* (1993). We recognize the model results as worth analyzing in detail, and will proceed to the investigation on the seasonal variation in the next chapter.

References

Anderson, L. A. and J. L. Sarmiento (1995): Global ocean phosphate and oxygen simulaions. *Glob. Biogeochem. Cycles*, **9**, 621–636.

Anderson, G. C., R. K. Lam, B. C. Booth and J. M. Glass (1977): A description and numerical analysis of the factors affecting the processes of production in the Gulf of Alaska. University of Washington, Department of Oceanography Special Report 76 (Reference M-77-40) 231 pp.

Antoine, D. and A. Morel (1996): Oceanic primary production 2. estimation at global scale from satellite (coastal zone color scanner) chlorophyll. *Glob. Biogeochem. Cycles*, **10**, 57–69.

Bacastow, R. and E. Maier-Reimer (1990): Ocean-circulation model of the carbon cycle. *Clim. Dyn.*, **4**, 95–125.

Bacastow, R. and E. Maier-Reimer (1991): Dissolved organic carbon in modeling oceanic new production. *Glob. Biogeochem. Cycles*, **5**, 71–85.

Beamish, R. J. and D. R. Bouillon (1993): Pacific salmon production trends in relation to climate. *Can. J. Fish. Aquat. Sci.*, **50**, 1002–1016.

Behrenfeld, M. J. and P. G. Flakowski (1997): Photosynthetic rates derived from satellite-based chlorophyll concentration. *Limnol. Oceanogr.*, **42**, 1–20.

Bidigare, R. R. and M. E. Ondrusek (1996): Spatial and temporal variability of phytoplankton pigment distributions in the central equatorial Pacific Ocean. *Deep-Sea Res. II*, **43**, 809–833.

Bogorov, V., M. D. Vinogradov, N. M. Voronina, I. P. Kanaeva and I. A. Svetova (1968): Distribution of zooplankton biomass within the surficial layer of the world ocean. *Dok. Akad. Nauk SSSR*, 1205–1207.

Brodeur, R. D. and D. M. Ware (1992): Long-term variability in zooplankton biomass in the subarctic pacific ocean. *Fish. Oceanogr.*, **1**, 32–38.

Bryan, K. (1984): Accelerating the convergence to equilibrium of ocean-climate models. *J. Phys. Oceanogr.*, **14**, 666–673.

Bryden, H. L. and E. C. Brady (1989): Eddy momentum and heat fluxes and their effects on the circulation of the equatorial Pacific Ocean. *J. Mar. Res.*, **47**, 55–79.

Chavez, F. P. and S. L. Smith (1995): Biological and chemical consequences of open ocean upwelling. p. 149–169. In *Upwelling in the Ocean: Modern Processes and Ancient Records*, ed. by C. P. Summerhayes, K.-C. Emeis, M. V. Angel, R. L. Smith and B. Zeitzschel, John Wiley & Sons.

Chavez, F. P., K. R. Buck, R. R. Bidigare, D. M. Karl, D. Hebel, M. Latasa, L. Campbell and J. Newton (1995): On the chlorophyll *a* retention properties of glass-fiber GF/F filters. *Limnol. Oceanogr.*, **40**, 428–433.

Chavez, F. P., K. R. Buck, S. K. Service, J. Newton and R. T. Barber (1996): Phytoplankton variability in the central and eastern tropical Pacific. *Deep-Sea Res. II*, **43**, 835–870.

Cox, M. D. (1987): Isopycnal diffusion in a z-coordinate ocean model. *Ocean Modelling*, **74**, 1–5.

Eppley, R. W. (1972): Temperature and phytoplankton growth in the sea. *Fish. Bull.*, **70**, 1063–1085.

Falkowski, P. G. and C. Wilson (1992): Phytoplankton productivity in the North Pacific ocean since 1900 and implications for absorption of anthropogenic CO_2. *Nature*, **358**, 741–743.

Fasham, M. J. R., J. L. Sarmiento, R. D. Slater, H. W. Ducklow and R. Williams (1993): Ecosystem behavior at Bermuda Station S and Ocean Weather Station INDIA: an observational analysis. *Glob. Biogeochem. Cycles*, **7**, 379–415.

Glover, D. M., J. S. Wroblewski and C. R. McClain (1994): Dynamics of the transition zone in coastal zone color scanner-sensed ocean color in the North Pacific during oceanographic spring. *J. Geophys. Res.*, **99**, 7501–7511.

Gordon, H. R., D. K. Clark, J. W. Brown and R. H. Evans (1982): Satellite measurements of the phytoplankton pigment concentration in the surface waters of a warm core Gulf Stream ring. *J. Mar. Res.*, **40**, 491–502.

Halpern, D., R. A. Knox, D. S. Luther and S. G. H. Philander (1989): Estimates of equatorial upwelling between 140° and 110°W during 1984. *J. Geophys. Res.*, **94**, 8018–8020.

Harrison, W. G., L. R. Harris and B. D. Irwin (1996): The kinetics of nitrogen utilization in the oceanic mixed layer: Nitrate and ammonium interactions at nanomolar concentrations. *Limnol. Oceanogr.*, **41**, 16–32.

Hellerman, S. and M. Rosenstein (1983): Normal monthly wind stress over the world ocean with error estimates. *J. Phys. Oceanogr.*, **13**, 1093–1104.

Hirst, A. C. and W. Cai (1994): Sensitivity of a world ocean GCM to changes in subsurface mixing parameterization. *J. Phys. Oceanogr.*, **24**, 1256–1279.

Ishizaka, J. and K. Ishikawa (1991): Northwest Pacific Carbon Cycle Study (NOPACCS) - MITI. *La Mer*, **29**, 152–154.

Ishizaka, J., H. Kiyosawa, K. Ishida, K. Ishikawa and M. Takahashi (1994): Meridional distribution and carbon biomass of autotrophic picoplankton in the Central North Pacific Ocean during Late Northern Summer 1990. *Deep-Sea Res.*, **41**, 1745–1766.

Kantha, L. H. and C. A. Clayson (1994): An improved mixed layer model for geophysical applications. *J. Geophys. Res.*, **99**, 25,235–25,266.

Killworth, P. D. (1996): Time interpolation of forcing fields in ocean models. *J. Phys. Oceanogr.*, **26**, 136–143.

Kirchamn, D. L., C. Lancelot, M. Fasham, L. Legendre, G. Radach and M. Scott (1993): Dissolved oragnic matter in biogeochemical models of the ocean. p. 209–225. In *Towards a Model of Ocean Biogeochemical Processes*, ed. by G. T. Evans and M. J. R. Fasham, Splinger.

Levitus, S. and T. P. Boyer (1994): *World Ocean Atlas 1994*, NOAA Atlas NESDIS 4, NODC.

Levitus, S., M. E. Conkright, J. L. Reid, R. G. Najjar and A. Mantyla (1993): Distribution of nitrate phosphate and silicate in the world oceans. *Prog. Oceanog.*, **31**, 245–273.

Longhurst, A., S. Sathyendranath, T. Platt and C. Caverhill (1995): An estimate of global primary production in the ocean from satellite radiometer data. *J. Plankton Res.*, **17**, 1245–1271.

Martin, J. H., G. A. Knauer, D. M. Karl and W. W. Broenkow (1987): VERTEX: Carbon cycling in the northeast Pacific. *Deep-Sea Res.*, **34**, 267–285.

Mellor, G. L. and T. Yamada (1982): Development of a turbulence closure model for geophysical fluid problems. *Rev. Geophys. Space Phys.*, **20**, 851–875.

Najjar, R. G., J. L. Sarmiento and J. R. Togweiler (1992): Downward transport and fate of organic matter in the ocean: Simulation with a general circulation model. *Glob. Biogeochem. Cycles*, **6**, 45–76.

Nitta, T. and S. Yamada (1989): Recent warming of tropical sea surface temperature and its relationship to the northern hemisphere circulation. *J. Meteor. Soc. Japan*, **67**, 375–383.

NOPACCS (1992): Cruise report of the Hakurei Maru cruise NH-02-2. Technical report, New Energy and Industrial Technology Development Organization.

Polovina, J. J., G. T. Mitchum and G. T. Evans (1995): Decadal and basin-scale variation in mixed layer depth and the impact on biological production in the Central and North Pacific, 1960-88. *Deep-Sea Res.*, **42**, 1701–1716.

Redi, R. H. (1982): Oceanic isopycnal mixing by coordinate rotation. *J. Phys. Oceanogr.*, **12**, 1154–1158.

Reid, J. L. (1962): On curculation, phosphate-phosphorus content, and zooplankton volumes in the upper part of the Pacific ocean. *Limnol. Oceanogr.*, **7**, 287–306.

Roemmich, D. and J. McGowan (1995): Climatic warming and the decline of zooplankton in the California Current. *Science*, **267**, 1324–1325.

Rosati, A. and K. Miyakoda (1988): A general circulation model for upper ocean simulation. *J. Geophys. Res.*, **18**, 1601–1626.

Sarmiento, J. L. and J. C. Orr (1992): A perturbation simulation of CO_2 uptake in an ocean general circulation model. *J. Geophys. Res.*, **97**, 3621–3645.

Sarmiento, J. L., R. D. Slater, M. J. R. Fasham, H. W. Ducklow, J. R. Toggweiler and G. T. Evans (1993): A seasonal three-dimensional ecosystem model of nitrogen cycling in the North Atlantic euphotic zone. *Glob. Biogeochem. Cycles*, **7**, 417–450.

Venrick, E. L., J. A. McGowan, D. R. Cayan and T. L. Hayward (1987): Climate and chlorophyll a: Long-term trends in the central North Pacific Ocean. *Science*, **238**, 70–72.

Wyrtki, K. (1975): Fluctuations of the dynamic topography in the Pacific Ocean. *J. Phys. Oceanogr.*, **5**, 450–459.

Yamanaka, Y. and E. Tajika (1996): The role of the vertical fluxes of particulate organic matter and calcite in the oceanic carbon cycle: Studies using an ocean biogeochemical general circulation model. *Glob. Biogeochem. Cycles*, **10**, 361–382.

Yoder, J. A., C. R. McClain, G. C. Feldman and W. E. Esaias (1993): Annual cycles of phytoplankton chlorophyll concentrations in the global ocean. *Glob. Biogeochem. Cycles*, **7**, 181–193.

Chapter 4

Characteristics of the seasonal variation of chlorophyll in the three-dimensional model

4.1 Introduction

Temporal variations of the oceanic ecosystem are affected by various factors. Vertical mixing, temperature, light intensity, nutrient composition, and species composition are, among others, especially important when we seek the cause(s) for variations of the oceanic ecosystem regardless of their temporal and/or spatial scale. Their effects on the ecosystem are most clearly seen in its seasonal variations. For instance, vernal blooming, which is a conspicuous feature in some oceanic regions, the North Atlantic, Bering Sea, *etc.*, is often associated with changes in the strength of vertical mixing (*e.g.*, Sverdrup, 1953; Evans and Parslow, 1985; Fasham, 1995); the summer maximum of plankton biomass in the California upwelling region has been explained by the fact that the upwelling becomes strongest in that season (*e.g.*, Thomas *et al.*, 1994); seasonal variations in High Nutrient - Low Chlorophyll (HNLC) regions might be strongly controlled by silicate (Dugdale *et al.*, 1995) or iron (Martin and Fitzwater, 1988) concentration. Therefore, understanding the mechanisms of seasonal variations will lead to grasping essential features of the oceanic ecosystem.

Seasonal features of the oceanic ecosystem show different patterns depending on the geographical position of the ocean. Colebrook (1979) demonstrated, by analyzing data in the North Atlantic obtained by the Continuous Plankton Recorder (CPR), that there are distinct differences in timing of the vernal blooming depending on the location. Us-

ing chlorophyll data from satellite measurements by Coastal Zone Color Scanner (CZCS), Longhurst (1995) divided the world ocean into 56 provinces which can be classified into four main domains, and showed typical patterns of seasonal variation in some of the provinces. Banse and English (1994) also used CZCS data to demonstrate the diversity of seasonal variations.

Many investigators attribute the geographical differences in seasonal variation to physical environments, although some attribute them to differences in chemical and/or biological conditions. Indeed, Colebrook (1979) related timing of the spring bloom to that of the sea surface warming based on the *in situ* data in the North Atlantic; Obata *et al.* (1996) also showed, on the global scale, the spring bloom is tightly related to the surface warming in the timing using the CZCS data and results from an ocean general circulation model (OGCM); Longhurst (1995) obtained 56 provinces based mainly on physical environments, adopting the notion that physics determines the overall feature of ecosystem behavior as a premise.

However, the extent to which physical environments can produce the diversity in seasonal variation, leaving chemical and/or biological processes out of consideration, has not been throughly examined. Here, we will investigate the role of physical environments in the oceanic ecosystem by using the OGCM with realistic seasonal variations. The North Pacific is the studying area.

Sarmiento *et al.* (1993) and Fasham *et al.* (1993) used the same kind of model, that is, an ecosystem model embedded in an OGCM, to investigate the ecosystem dynamics in the North Atlantic. Their main purpose was, however, to identify discrepancies of biomass distributions between model results and observations and to clarify the causes of the discrepancies. Seasonal variation in the model was not discussed in detail.

Some studies dealt in detail with the relation between differences in physical environments and seasonal variations of ecosystem. Evans and Parslow (1985) and Fasham (1995) demonstrated, using a box model, that the difference in the dynamics of the mixed layer can explain that between regions with and without a large spring bloom. McCreary *et al.* (1996) investigated seasonal variations in the Indian Ocean with an ecosystem model embedded in a 2.5 layer model of the ocean. They showed that the seasonal variations at some selected regions are deeply affected by the mixed layer depth (MLD). In the above mentioned papers, focuses are on the causes for formation of the seasonal variations at some chosen locations, but not on spatial extent of the region with the same seasonal variation. A next

step will be to classify all the seasonal variations in the whole domain, and then to identify the physical mechanism(s) playing a central role in determining the spatial distribution of the seasonal variation patterns.

In this chapter, by analyzing the results of the combined model, *i.e.*, the three-dimensional ecosystem model embedded in the OGCM for the North Pacific in Chapter 3, we will identify the seasonal patterns and their spatial distribution which emerge in the model to examine how physical environments regulate seasonal variations of the ecosystem. In Section 4.2, the domain is divided into seven areas based on the seasonal variation patterns and the annual mean abundance of chlorophyll. It will be shown that the pattern and the extent of each area are well compared to the observations. The mechanisms forming the contrasts of such patterns in the model are then investigated in Section 4.3. The factors determining the overall distribution of the seasonal patterns are discussed in Section 4.4. Finally, summary and conclusion are provided in Section 4.5.

We use the model data obtained in the Chapter 3, where the model performance has been extensively examined. In Chapter 3, the model results for physical fields, nitrate, chlorophyll, zooplankton, and primary production were compared with the observations on the spatial scale of the North Pacific basin. In addition, the mechanisms determining the distribution of the primary production was also investigated. Thus, in the previous chapter, it was proved that the model products are not unrealistic and worth analyzing.

4.2 Areal division of the domain

As explained in the previous chapter, all data for the analysis are the monthly averages in the sixth year of the integration; the twelve datasets comprise the annual cycle.

4.2.1 Procedure of the areal division and description of each area

To obtain characteristic seasonal variation patterns and their distribution, Empirical Orthogonal Function (EOF) analysis is applied to chlorophyll (strictly equivalent to phytoplankton in the model) data averaged over the upper 150 m. In the analysis, data at latitudes higher than 52°N are excluded, because too many modes are needed only to explain the variation in the high latitude region; amplitudes of seasonal variations are far larger in the high latitude region as shown later. Data near the southern artificial wall,

23°S - 11°S, are also excluded.

The first two principal modes are displayed in Fig. 4.1 with their time coefficients. The first mode (EOF 1) shows that the amplitude of seasonal variations is higher in the middle and high latitude regions. It reaches its maximum phase in April. The peaks in the second mode (EOF 2) are located where the mixed layer becomes extremely deep in early spring (Fig. 3.4). The phase is opposite between the area off Sanriku coast and the one along the latitudinal line of about 30°N.

The information from the EOF analysis is utilized for the areal division of the domain. The annual mean abundance of chlorophyll averaged over the upper 150 m (Fig. 4.2) is also exploited because it is highly probable that, even if the seasonal patterns look alike, they are formed by different mechanisms in a eutrophic, chlorophyll-rich region and an oligotrophic, chlorophyll-poor region.

Thus, an areal division is created as shown in Fig. 4.3 based on the EOF modes and the annual mean abundance. The areas are named by two alphabets. The origins of the names are given in Table 4.1 along with the characteristic features of the areas. Regions of sharp fronts in Fig. 4.2 are not included in the division but treated as transition zones except the area KS where the front itself constitutes modal peaks. Each area contains one of the peaks in either the EOF modes or the annual mean abundance. Also, each boundary between the areas corresponds to a front in either the EOF modes or the annual mean abundance. Thus, this division is a highly objective one based only on the chlorophyll data in the model.

Table 4.1. Features of the areas shown in Fig. 4.3

Name of the area	Feature
BO (Bering & Okhotsk Sea)	Extremely large amplitude of seasonal variation
SP (SubPolar region)	Positive peak in EOF 1
PR (Purturbed Region)	Positive peak in EOF 2
CU (Coastal Upwelling region)	High abundance in annual mean
KS (KuroShio & Kuroshio Extension)	Negative peak in EOF 2
ST (SubTrophical region)	Low abundance in annual mean
EQ (EQuatorial region)	High abundance in annual mean

There are distinct differences in the seasonal patterns among the areas as shown in Fig.

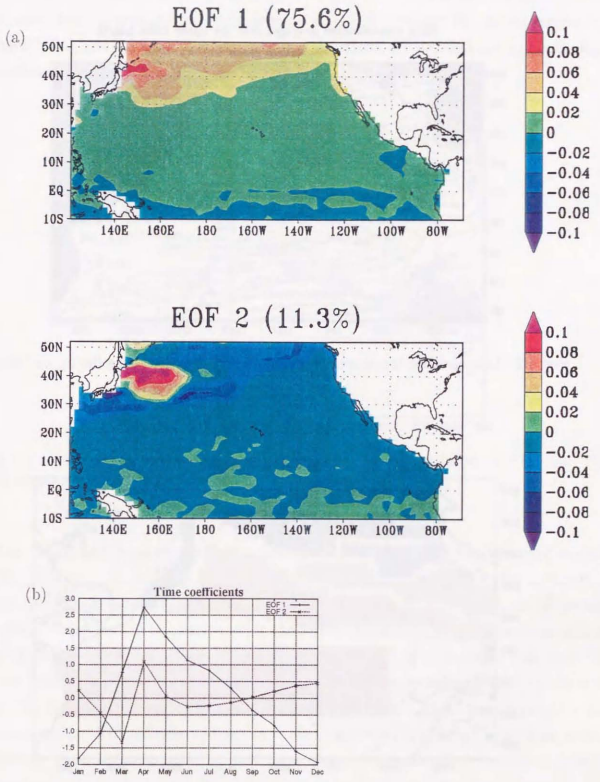

Fig. 4.1. (a) First two principal modes of the EOF analysis applied to model chllorophyll data averaged over the upper 150 and (b) their time coefficients. In the parentheses of (a) are the percentages by which the total variance is accounted for. In (b), the solid line represents the time coefficients for the first mode and dashed line for the second mode.

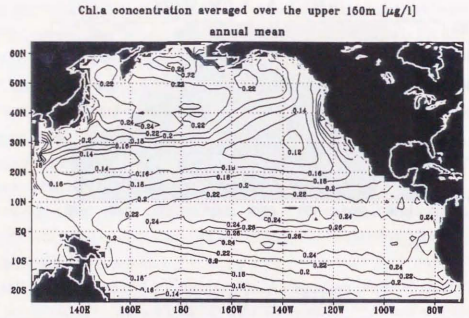

Fig. 4.2. Annual mean concentration of chlorophyll averaged over the upper 150 m.

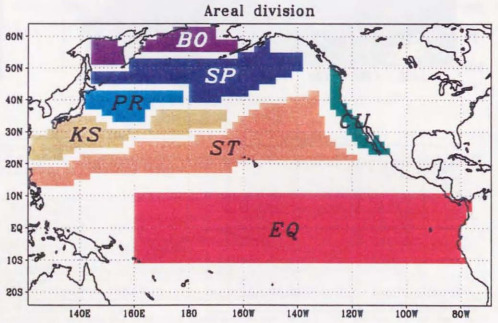

Fig. 4.3. Areal division of the domain based on the model.

4.4, which represents the seasonal variations averaged over the area and the upper 150 m. It is seen that the area BO has the maximum amplitude. PR has the second largest one while SP, CU, and KS show moderate seasonal variations. ST and EQ indicate only slight variations.

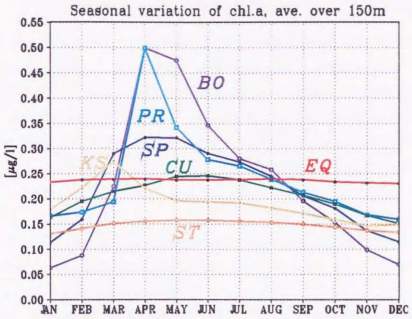

Fig. 4.4. Modeled seasonal variation of chlorophyll in each area shown in Fig. 4.3. The data are averaged over each area and the upper 150 m.

Figs. 4.5(a) and (b) show seasonal variations of MLD and nitrate to understand what is taking place in the model. PR and KS go through large variations of MLD due to the effect of the Kuroshio in the model, reaching their maximum phase in early spring; the impacts of the MLD variations can be clearly seen in the nitrate, meaning that the ecosystems will be also affected by the MLD variations. ST is nitrate depleted all through the year (here the phrase "nitrate depleted" means that the surface nitrate concentration is of the order of or less than the value of the half saturation constant for nitrate, which is 0.03 μmol/l). KS becomes nitrate depleted from summer to fall but relatively enriched in nitrate from winter to spring. The other areas never become nitrate depleted because all of them are located in regions with wind-induced upwelling, which brings nitrate from under the euphotic zone; it is worth pointing out that ST and KS lie in an area with wind-induced downwelling. The relation between the seasonal variations of the model chlorophyll and the factors such as

MLD, upwelling, and nitrate concentration will be discussed more in detail in Sections 4.3 and 4.4.

4.2.2 Comparison with observations

Comparison with an areal division based on observations

Fig. 4.6 depicts the ecological areal division for the North Pacific proposed by Longhurst (1995). This figure is created based on observations, and is used to classify seasonal variations of chlorophyll detected by CZCS (Longhurst, 1995), as well as to describe the variation of parameters for estimating primary production from CZCS data (Longhurst *et al.*, 1995). A remarkable resemblance can be found between this figure and the model result in Fig. 4.3. BERS in the former corresponds to BO in the latter, PSAG(W) and PSAG(E) to SP, KURO to PR, NPST(W) to KS, NPST(E) and NPTG to ST, and PNEC together with PEQD to EQ. Although each of the model areas SP, ST, and EQ contains two areas of the observation, similarity can be found between the two of each combination: the shallow haloclines found in both NPST(E) and NPST(W) bring impacts on the ecosystem there; in both NPST(E) and NPTG, deep subsurface chlorophyll maxima are formed throughout the year at depths deeper than 100 m, thus indicating a feature of oligotrophic regions; wind-induced upwelling occurring in both PNEC and PEQD transports nutrients to enhance biological activities (Longhurst, 1995). The striking agreement between Fig. 4.3 and Fig. 4.6 lends some support to the reality of the seasonal variations in the model.

4.2.3 Comparison with satellite data

In Fig. 4.7, model chlorophyll concentrations in each area are compared with those detected by CZCS. The satellite data are also averaged over each area shown in Fig. 4.3. As stated in Chapter 3, the satellite observation provides information averaged over the depth of the order of only 10 m (*e.g.*, Gordon *et al.*, 1982). Therefore the model seasonal variations are replotted using data averaged over the upper 10 m so that they can be directly compared to the CZCS data. The satellite data in high latitude regions for October - February are excluded because they are distinctly unreliable (Yoder *et al.*, 1993).

It is very easy to find differences between the two figures, but yet many common features are found:

- The amplitude in BO is much larger than that of any other area;

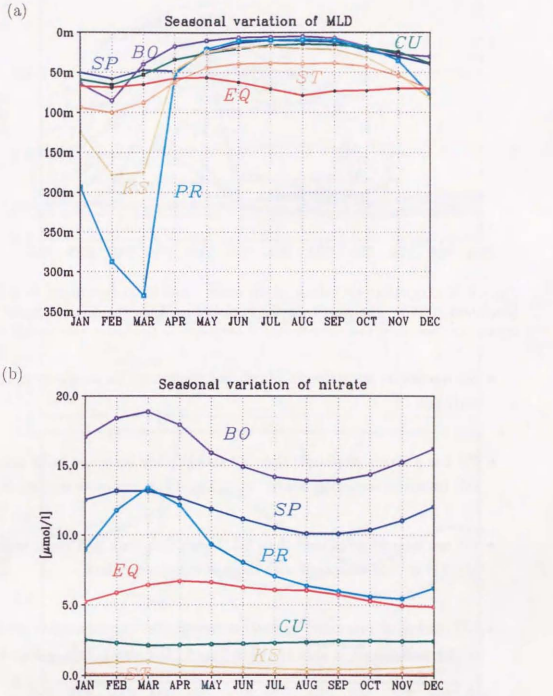

Fig. 4.5. Modeled seasonal variations of (a) MLD and (b) nitrate, as averaged over the area shown in Fig. 4.3. Nitrate data are averaged over the upper 100 m.

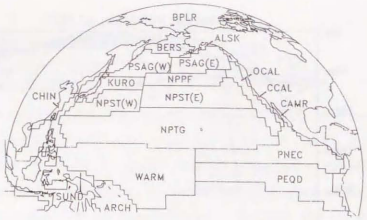

Fig. 4.6. Ecological areal division of the ocean based on observational facts (redrawn from Longhurst, 1995). The North Pacific is picked up from the original figure for the world ocean.

- KS reaches its maximum in March and declines to its minimum in late summer or early fall;
- PR has a larger amplitude than SP though they lie in the same range of latitude; this feature is somewhat wiped out in Fig. 4.7(a) but quite noticeable in Fig. 4.4;
- PR has a larger amplitude than KS though they both go though large variations of MLD (Fig. 4.5) compared with those in the other regions;
- CU reaches its maximum in summer though the concentration is much lower in the model; this feature is hard to tell in Fig. 4.7 but clearly seen in Fig. 4.4;
- ST and EQ experience very small variations.

These agreements are striking considering the simplicity of the ecosystem model and the fact that the areal division is totally based on the model chlorophyll data.

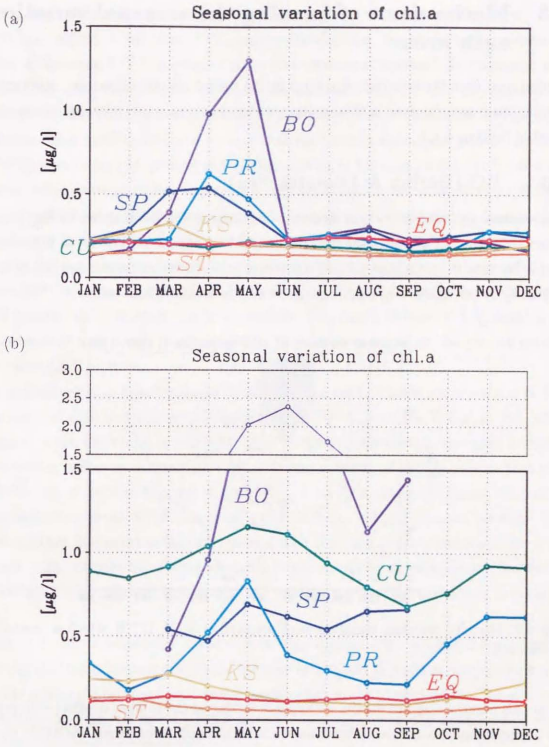

Fig. 4.7. Seasonal variation of chlorophyll averaged over the area shown in Fig. 4.3 for (a) model data averaged over the surface 10 m and (b) CZCS data. The CZCS data in high latitude regions for October - February are not shown because they contain large error.

4.3 Mechanisms of forming the seasonal variation of each area

Having seen that the seasonal variations in the model are not unrealistic, mechanisms of forming them are examined in this section with emphasis on points related to the similarities listed in Section 4.2.3.

4.3.1 BO (Bering & Okhotsk Sea)

The seasonal variation of vertical structure of chlorophyll in BO is shown in Fig. 4.8. Here, instead of taking an average over the area, a specific point (56°N, 177°W) in BO is selected. This is because the averaging process sometimes obscures characteristic features of interest, especially in the analysis of term balance, which is actually done below.

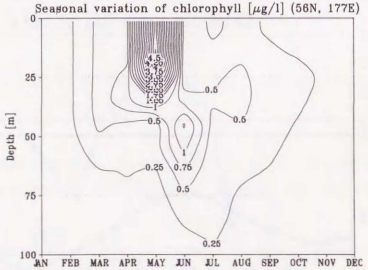

Fig. 4.8. Modeled seasonal variation of chlorophyll at 56°N, 177°E, which is located in BO in Fig. 4.3.

At this point, a distinct maximum appears in May at the shallow depths ($\sim$ 10 m). After its disappearance, a relatively weak subsurface chlorophyll maximum (SCM) is formed at deeper depths, being clearest in June. In winter, the concentration becomes smaller and independent of depth.

The high concentration in May has supporting evidence not only from the CZCS data (Fig. 4.7), but also from the *in situ* data of Smith and Vidal (1984) who observed the

extremely high chlorophyll concentration ($\sim$ 10μmol/l) in May at several stations. How is the bloom excited in the model? To answer the question, the terms in the governing equation of chlorophyll (2.21) acting in the water column are averaged over a month and plotted in Fig. 4.9. The balances are shown for April and May because they correspond to, respectively, immediately before and at the maximum phase of the bloom. In April, the contribution from vertical mixing is so large that the balance against net primary production (NPP) is supported by grazing and vertical mixing at the depth where NPP takes the maximum value; vertical mixing is playing a significant role in sweeping chlorophyll away from the most suitable place for photosynthesis. In contrast, the contribution from vertical mixing is very small in May; the overall balance is kept between NPP and grazing. This qualitative difference in term balance between April and May means that a large imbalance between NPP and grazing is produced by surface warming and subsequent weakening of vertical mixing; the imbalance works to increase chlorophyll because it is generated by disappearance of a term acting against NPP. The bloom ceases when the grazing catches up the chlorophyll increase.

The summer SCM is formed mainly by the effect of light. This is made evident in Fig. 4.10 where the light dependence of photosynthesis ($[I/I_{opt}]\exp[1 - I/I_{opt}]$ in Eq. (2.1) averaged over the day cycle) is plotted *. Due to the photoinhibition, the most favorable light condition occurs at a depth of $\sim$ 40 m during summer. This depth is located very close to the one of SCM in Fig. 4.8, suggesting that the light condition is most responsible for the formation of the SCM. The small differences in depth of maxima between Figs. 4.8 and 4.10 are due to other factors, among which the ammonium inhibition is the most dominant. The summer SCM after blooming is also found in an observation (Sambrotto and Goering, 1983), although it is hard to tell whether the forming mechanism is the same or not.

In Fig. 4.8, the extreme value exists only in May while in Figs. 4.4 and 4.7(a) it is also seen in April. This is because the maximum may be reached in April at some other points where the retreat of the mixed layer occurs earlier than at the present point. The shapes of the variations in Figs. 4.4 and 4.7 result from the integration over the grids each of which

*Strictly speaking, the plotted values of each month are monthly averaged photosynthesis divided by $[\{NO_3/(NO_3 + K_{NO3})\}\exp(-\Psi NH_4) + NH_4/(NH_4 + K_{NH4})]\exp(kT)$Chl (see Section 2.2.1 and Table 2.1 for the notations), where monthly mean values are used for each variable. Therefore, they may contain significant error when the time evolution rates of the variables become large. This is evidenced in the peculiar maximum in January in Fig. 4.20 (a), which appears later. This kind of plotting is, however, enlightening if enough care is taken over the point.

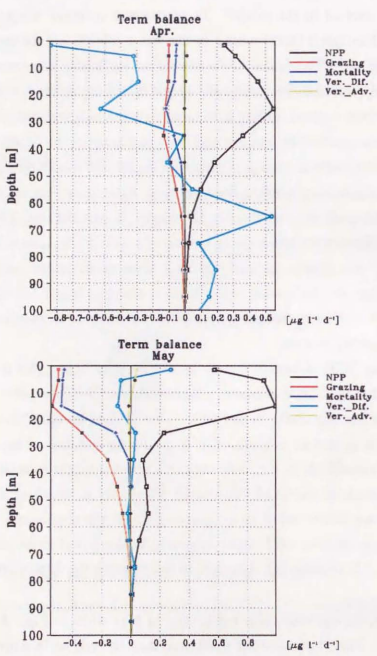

Fig. 4.9. Balance among the selected terms in the governing equation of chlorophyll (2.1) for (a) April and (b) May at 56°N, 177°E. The terms for photosynthesis and respiration are combined as NPP (net primary production) for simplicity. Black line represents NPP, red grazing, blue mortality, yellow vertical advection, and light blue vertical diffusion. Horizontal scaling is different between the two plots to enlighten the relative contribution of each term.

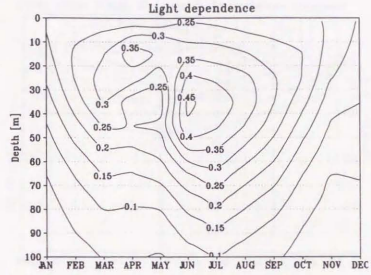

Fig. 4.10. Light dependece of photosynthesis at 56°N, 177°E. More specifically, a contour of $[I/I_{opt}]\exp[1 - I/I_{opt}]$ in Eq. (2.1) averaged over the day cycle.

takes the maximum value at different time in April or May.

The duration of the high chlorophyll concentration is not long enough in the model compared with the CZCS data. The reason for this disagreement is not clear. It may be that the shallowing of the mixed layer occurs as late as in June at some locations in reality. Another possibility is the succession of species caused by the variation of silicate concentration, which is not incorporated in the model; a bloom of dinoflagellates often takes over one of diatoms after silicate becomes depleted thereby making the apparent duration of the bloom longer (Tsunogai and Noriki, 1983).

4.3.2 SP (SubPolar region)

Seasonal variation of chlorophyll is shown in Fig. 4.11 for the point 48°N, 155°W, which is located in SP. No pronounced blooming can be found here despite that this region is located near BO, where chlorophyll concentration takes an extremely high value in April or May almost everywhere. This uniformity of chlorophyll concentration has been also observed at OWS Papa (Fig. 2.4), which is near the selected point †.

†The point exactly corresponding to OWS Papa is not chosen here because in the model it is located close to the transition zone between nitrate depleted (ST) and nitrate rich region (SP). In reality, however, the transition zone lie far more south than in the model, so that OWS Papa can be safely considered as in a nitrate rich region.

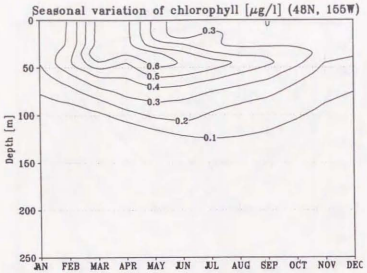

Fig. 4.11. Modeled seasonal variation of chlorophyll at 48°N, 155°W, which is located in SP in Fig. 4.3.

The reason for the absence of blooming can be seen in Fig. 4.12, where water column term balance at the point is shown for March. Even in this month when vertical mixing is most vigorous here, the contribution from vertical mixing is small at the depth of the maximal NPP compared with the one in the case of BO (Fig 4.9). Thus the grazing term can be in balance against NPP almost all through the year thereby suppressing bloom. In turn, the inhibition of strong vertical mixing is caused by strong stratification due to a shallow halocline. This is made evident in Fig.4.13 which represents the vertical profiles of potential density, temperature, and salinity in March. It can be seen that the halocline at a depth of 40 m is so steep as to prevent convection due to the surface cooling suggested in the figure. The suppression on deepening of the mixed layer by the shallow halocline has been also pointed out by many observational studies (*e.g.*, Tabata, 1964) though it lies at a deeper depth ($\sim$ 100 m) according to observation. Furthermore, the banning of a bloom by shallow winter mixed layer in the subarctic Pacific is also suggested by other modeling studies (Evans and Parslow, 1985; Fasham, 1995).

The halocline exists throughout the area SP but it suddenly declines at the boundary between SP and BO. This is clearly seen in Fig. 4.14(a); north of $\sim$ 54°N where the boundary is located, the halocline looses its steepness. This distinct difference in salinity structure induces the contrast in the seasonal variations of SP and BO. The tendency of

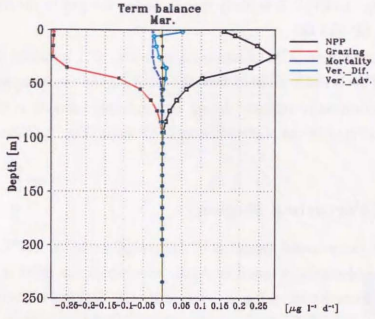

Fig. 4.12. As in Fig. 4.9 but for March at 48°N, 155°W.

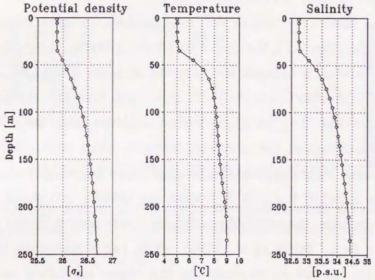

Fig. 4.13. Profiles of potential density, temperature, and salinity in March at 48°N, 155°W.

the halocline to rapidly decline toward the north is also seen in the data of Levitus and Boyer (1994) (Fig. 4.14(b)). It is likely that in reality the gap in the halocline also causes the difference in SP and BO.

Besides, the pronounced SCM in summer seen in Fig. 4.11 is formed by the same mechanism as in BO. This is easily inferred from the fact that the two areas are both nitrate rich so that the only process to strongly inhibit phytoplankton growth is the photoinhibition. The SCM is also found in the observation at OWS Papa (Fig. 2.4) though the strength is much weaker.

4.3.3 PR (Perturbed Region)

Fig. 4.15 shows the seasonal variation of chlorophyll at 38°N, 157°E. As in the case of BO, conspicuous blooming is found in April, after which the SCM is formed. The high chlorophyll concentration in spring is detected by CZCS (Fig. 4.7) and also seen in Imai *et al.* (1988), who compiled *in situ* data from 1973 to 1984 taken by the quarterly routine observation around Japan.

The resemblance between PR and BO is also retained even if we look into the mechanism of shaping the seasonal variations. The term balances shown in Fig. 4.16 tell the same story to that of BO; surface warming causes an imbalance between NPP and grazing, and thus it results in the rapid phytoplankton growth.

A care must be taken even though the model seasonal variation looks very similar to the satellite observation (Fig. 4.7); the deep mixed layer in March, the cause for the pronounced blooming in this model, is brought about by the inability of the OGCM to reproduce the separation of the Kuroshio (Chapter 3). In reality too, however, the mixed layer in March is deep in this area (Fig. 3.4) though somewhat shallower than that in the model. The real oceanographic conditions in this area are, however, much more complicated than in the model: the Kuroshio separates from the coast of Japan far more south; interactions among warm core rings detached from the Kuroshio, the Oyashio intrusions, and heat and fresh water exchange between the atmosphere and the ocean determine the density structure in the surface layer (*e.g.*, Talley *et al.*, 1995), which has a drastically large time variation. These interactions can not be expressed in this coarse resolution model. Therefore, the processes of the mixed layer deepening in the model and the real world differ, but yet the results are similar. It is probable that the real blooming is also excited by this deep mixed layer.

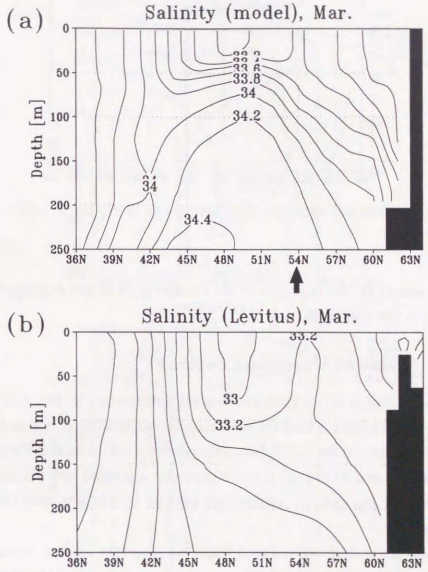

Fig. 4.14. Salinity in March along 179°W for (a) the model and (b) the observation (Levitus and Boyer, 1994). The arrow in (a) indicates the location of the boundary between SP and BO.

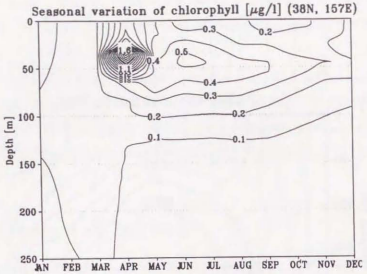

Fig. 4.15. Modeled seasonal variation of chlorophyll at 38°N, 157°E, which is located in PR in Fig. 4.3.

Besides, the reason for the existence of the summer SCM is also explained by the photoinhibition, as in the case of BO and SP.

4.3.4 CU (Coastal Upwelling region)

Chlorophyll concentration shows a modest seasonal variation in CU (Fig. 4.17 for the point at 36°N, 125°W). The feature that the chlorophyll concentration is high in early summer corresponds to that seen in the CZCS data although the absolute value of the concentration is much lower in the model (Fig. 4.7), and is indirectly supported by Chelton *et al.* (1982), who showed that *in situ* data of zooplankton biomass in this area take their maximum value in summer.

Due to the absence of deep vertical mixing and the abundant nutrient transported by the wind-induced upwelling, the chlorophyll concentration closely traces the variation of light condition (Fig. 4.18), which provides the most favorable condition in June. It is worth pointing out that the best condition in June is brought about not by the intense light, but the long duration of daytime; the daily averaged light intensity at the sea surface is well above the optimal light intensity (I_{opt} in Eq. (2.1)) all through the year, which is readily inferred from Fig. 4.18 where the light condition is most suitable for photosynthesis always at the subsurface, implying that the surface light is more intense than the value of I_{opt}.

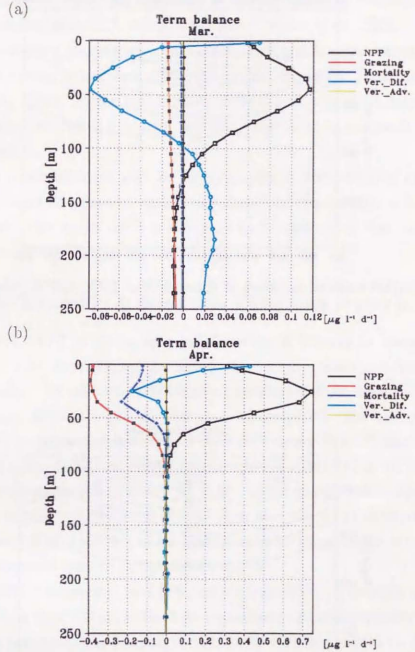

Fig. 4.16. As in Fig. 4.9 but for (a) March and (b) April at 38°N, 157°E. Horizontal scaling is different between the two figures to enlighten the relative contribution of each term.

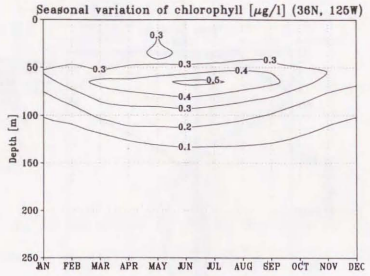

Fig. 4.17. Modeled seasonal variation of chlorophyll at 36°N, 125°W, which is located in CU in Fig. 4.3.

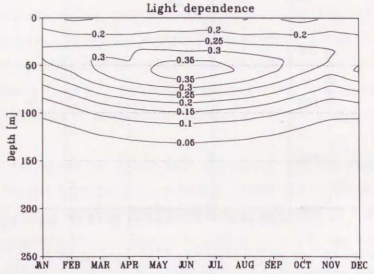

Fig. 4.18. As in Fig. 4.10 but for the point 36°N, 125°W.

Contrary to the model results, high chlorophyll concentration in summer is often associated with the seasonal variation of upwelling intensity in observational studies (Mann and Lazier, 1991). But in fact, the explanation that the upwelling intensity determines the chlorophyll seasonal variation is still a hypothesis (Thomas *et al.*, 1994).

The low chlorophyll concentration is perhaps attributable to the parameter choice. It is known that neritic species have more vigorous photosynthetic rates than oceanic ones (Parsons *et al.*, 1984). In the model, the photosynthetic rate characteristic for oceanic species is applied all over the domain and this value must be too small for the coastal upwelling region.

Though the concentration is low, the model amplitude of the seasonal variation relative to the annual mean abundance is rather large (amplitude/mean ratio ~ 0.4 as calculated from Fig. 4.4). The model result is indicative in demonstrating that the effect of light alone can generate such large annual variation.

4.3.5 KS (Kuroshio & Kuroshio Extension region)

The point 28°N, 141°E is chosen as a representative of KS and its seasonal variation is plotted in Fig. 4.19. From January to March, chlorophyll maximum is found at relatively shallow depths (0 - 60 m) with rather high concentration; from April to December, it is formed at deeper depths ($\sim$ 100 m) with lower concentration. The high concentration in winter or early spring is also seen well in the CZCS data (Fig. 4.7) and the observation of Imai *et al.* (1988). Longhurst (1995) suggests that in NPST(W) of his province division (Fig. 4.6) which corresponds to KS of this study, relatively high chlorophyll concentration is retained at the near-surface levels (0 - 50 m) in late winter and a deeper SCM is found in other seasons. The agreement of his description with the variation shown in Fig. 4.19 adds an observational basis to the model calculation.

The deep SCM is maintained by a different mechanism from that in the cases of BO and others. Shown in Fig. 4.20(a) is the light dependence of photosynthesis. It can be seen that the most favorable light condition occurs at far shallower depths ($\sim$ 50 m) than the SCM. This is because nitrate is depleted where light condition is optimal. Fig. 4.20(b) shows the nutrient dependence in the governing equation of chlorophyll ($[NO_3/\{NO_3 + K_{NO3}\}] \exp\{-\Psi NH_4\} + NH_4/\{NH_4 + K_{NH4}\}$ in Eq. (2.1)). It is clear that in summer, nutrient environment is so ill-conditioned at the depths of optimal light condition. The SCM forms where the product of the light dependence and the nutrient dependence takes

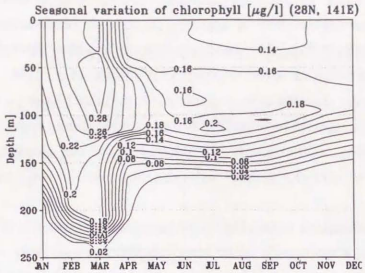

Fig. 4.19. Modeled seasonal variation of chlorophyll at 28°N, 141°E, which is located in KS in Fig. 4.3.

the maximum value; in other words, the SCM settles down at the depths where the light condition is balanced with the nutrient condition. The ultimate cause of the difference in the mechanism of SCM formation between KS and BO is the wind-induced vertical flow; KS is in the region with Ekman downwelling which strips nutrients of the surface layer, while BO is in the region with Ekman upwelling which supplies nutrients to the surface layer.

It can be also seen that from January to March, nitrate depletion is relaxed due to the deep vertical mixing. Phytoplankton growth is thus enhanced, and it results in the high concentration from late winter to early spring. It is interesting that the role of vertical mixing is totally reversed compared with that in the case of BO and others, where vertical mixing acts to reduce biological activities by damaging the light condition. On the contrary, here in KS where nitrate is exhausted during warm seasons, deepening of the mixed layer enhances photosynthesis by transporting nitrate to the surface layer. The deep mixed layer can be found also in the observation (Fig. 3.4). It is likely that the mechanism described above is in effect also in reality.

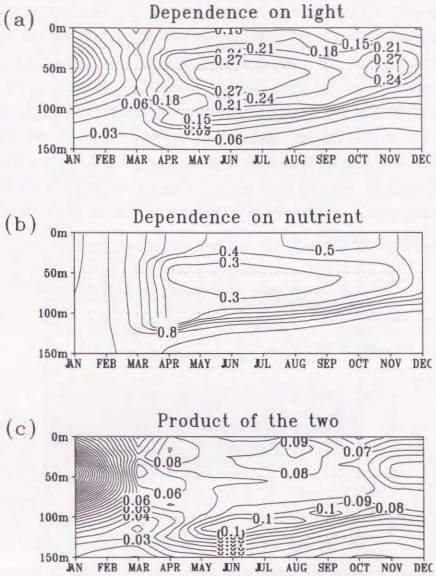

Fig. 4.20. Dependence of photosynthesis on (a) light and (b) nutrientat at 28°N, 141°E. More specifically, contours in (a) $[I/I_{opt}]\exp[1 - I/I_{opt}]$ and (b) $[NO_3/\{NO_3 + K_{NO3}\}]\exp\{-\Psi NH_4\} + NH_4/\{NH_4 + K_{NH4}\}$ in Eq. (2.1). The product of the two is also plotted in (c).

4.3.6 ST (SubTropical region)

Fig. 4.21 depicts the seasonal variation of chlorophyll at 26°N, 149°W. The deep SCM is formed throughout the year with modest maxima in March and May. The SCM is retained by the same process, *i.e.*, the balance between the light and the nutrient condition. The moderate variation is caused by the change in the intensity of light and vertical mixing: in March, the vertical mixing can reach to a depth of about 100 m, thereby stimulating the biological activities; in summer when the light is strong, the chlorophyll concentration is enriched because the light can penetrate more deeply so that the two conditions mentioned above can be balanced at deeper depths, where more abundant nitrate is available for photosynthesis. The maximum in summer is not in June when the light is strongest but in May. This is because in May, the effect of vertical mixing to bring nutrient to the surface layer still remains a little, so that the nutrient concentration at the depth of the SCM is slightly higher than in June.

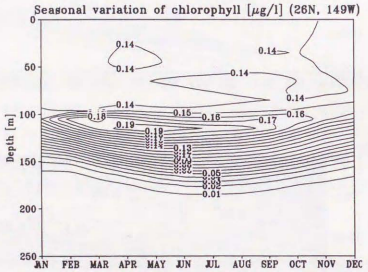

Fig. 4.21. Modeled seasonal variation of chlorophyll at 26°N, 149°W, which is located in ST in Fig. 4.3.

The seasonal variation of chlorophyll in the subtropical Pacific is extensively observed at Station ALOHA (23°N, 158°W) by the Hawaii Ocean Time-series (HOT) Program since October 1988 [‡]. The mean integrated chlorophyll abundance from 1988 to 1993 is provided

[‡]Here, the selected point is not at exactly the same place as Station ALOHA. This is because the

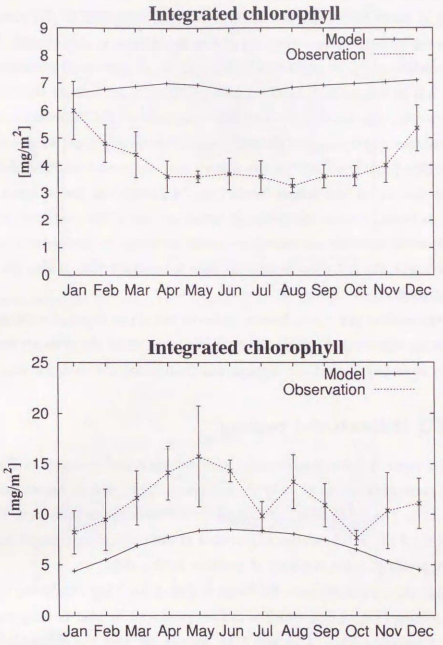

Fig. 4.22. Chlorophyll abundance integrated over (a) 0 - 50 m and (b) 100 - 175m. The model results (solid line) are taken from the point 26°N, 149°W, which is located in ST in Fig. 4.3. The observation (dashed line with errorbars) indicates the averaged values over 1988 through 1993 obtained in the HOT Project (Winn *et al.*, 1996). The errorbars show the standard deviation.

by Winn *et al.* (1996), and it is shown in Fig. 4.22 with the corresponding model results. Near the sea surface (Fig. 4.22(a)), the chlorophyll abundance is fairly constant in the model while it takes the minimum value in summer according to the observation. The summer low values in the observation are due to the increase in N/Chlorophyll ratio caused by the photoadaptation, as explained in Chapter 2. The seasonal variation near the sea surface can not be reproduced by the model which does not include the photoadaptation process. However, this fault might not be serious because the decreased chlorophyll does not reflect reduced phytoplankton biomass, which is more important for the biogeochemical cycle than chlorophyll itself is. On the other hand, the model and the observation show the common feature at the deeper levels (Fig. 4.22(b)) that the integrated chlorophyll increases in summer, though the modeled values are out of the ranges of errorbars. Winn *et al.* (1996) state that the increase does reflect a change in phytoplankton biomass and that it is brought about by the change in light intensity, which is also the cause for the modeled variation.

Besides, the modest maximum from summer to fall at the depth of $\sim$ 70 m is formed due to the nutrients regenerated within the euphotic zone, while the stronger maximum below is formed by spending the nitrate transported from under the euphotic zone by diffusion.

4.3.7 EQ (EQuatorial region)

EQ does not seem to have a systematic seasonal variation as shown in Fig. 4.23, where chlorophyll concentration at 0°, 139°W is plotted. This view is supported by the CZCS data (Fig. 4.7). The SCM in EQ is formed by the same mechanism as in BO and others, *i.e.*, the depth of the SCM corresponds to that of the optimal light condition; owing to the equatorial upwelling, there is plenty of nutrient in this area.

Small short term variations can be found in Fig. 4.23. They are caused by the variation in vertical mixing (Fig. 4.24), which is in turn produced by that in temperature and wind stress. By comparing Figs. 4.23 and 4.24, we can see that the chlorophyll maximum in May and June corresponds to the period when the vertical mixing is weak at the depth of the SCM and the minimum in November to that when it is strong; the vertical mixing acts to interfere with phytoplankton growth in this nutrient replete area.

position of Station ALOHA is located at the edge of ST in the model so that it may not be considered as a representative of the area. In reality, however, the station is well within the real counterpart of ST so that it can be regarded as a typical point in the subtropical oligotrophic ocean.

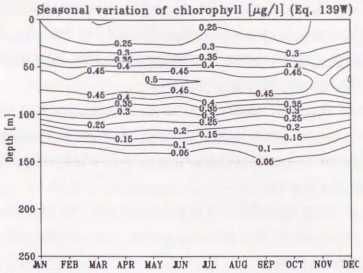

Fig. 4.23. Modeled seasonal variation of chlorophyll at 0°, 139°W, which is located in EQ in Fig. 4.3.

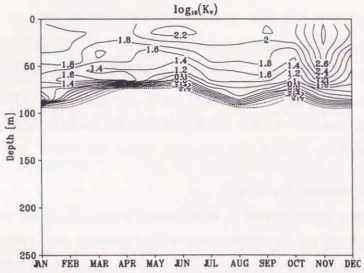

Fig. 4.24. Vertical diffusion coefficient (presented in common logarithm). The unit of the coefficient is in cm/sec^2.

4.4 Discussion

In the previous section, the mechanisms for shaping the seasonal pattern of each area are examined by selecting a specific point as a representative of the area. What determines the distribution of the patterns is, however, still not very clear. This section deals with the factors which draw the boundaries among the areas.

So far we have seen that the factors such as light, nutrient, and vertical mixing are combined in various ways to result in the diversity of seasonal variation. It is possible, however, to comprehensively classify the variations in terms of physical environments, which also define the extent of the area.

Obviously, seasonal variation of MLD should be included in the physical factors for the classification; large variations of MLD always result in corresponding chlorophyll variations as shown in the previous section.

To find other physical factors, it is helpful to remember that the ecosystem behavior shows remarkable differences between areas with replete nutrient and ones with limited nutrient. The influences of nutrient concentration can be summarized as below:

- abundance of phytoplankton:
  Phytoplankton is more abundant in the eutrophic region than in the oligotrophic region.

- how phytoplankton responds to changes in MLD;
  In the eutrophic region deepening of the mixed layer acts to suppress photosynthesis, while in the oligotrophic region it stimulates photosynthesis. This is because in the oligotrophic region the vertical mixing causes the nutrient supply rather than the chlorophyll dilution, while in the eutrophic region the reverse is true.

- mechanism of forming the SCM;
  In the eutrophic region, the SCM is located at the depth of the most favorable light condition, while in the oligotrophic region it is retained at the depth where the light and the nutrient condition are balanced.

- vulnerability of phytoplankton to changes in MLD.
  As explained above, the SCM is formed at the depth of the optimal light condition in the eutrophic region. This means that biological activities are vigorous at relatively shallow depths. Therefore, even if MLD is somewhat shallow, phytoplankton is subject to strong vertical mixing when the nutrient concentration is high.

The second and the fourth item are obviously related to the shape of the seasonal variations. Thus the nutrient concentration is a key to define it. The nutrient concentration is, in turn, tightly related to the vertical velocity, which means that the vertical velocity should be one of the physical factors for the classification.

Fig. 4.25 shows the relation among the areal division, the vertical velocity, and the seasonal variation of MLD. It is clearly seen that the contourlines of the vertical velocity and the amplitude of the MLD seasonal variation define the boundaries, except for EQ where the strong Ekman divergent flow spreads out the nutrient lifted up by the upwelling and the deep MLD (Fig. 3.4) is also acting to enrich the nutrient on both sides of the equator. Considering the fact that the areal division is made based only on the model chlorophyll data and no information from physical variables is utilized, the agreement between the boundaries and the contourlines is impressive.

On the basis of Fig. 4.25, the seven areas can be classified as in Fig. 4.26. Indeed, areas sorted in the same quadrant show similar seasonal variations. The resemblance between BO and PR has been, for example, already pointed out in Section 4.3.3; minor differences between the two areas are attributable to other various factors such as the differences in light and temperature. This diagram is demonstrating that the diversity in the seasonal variations of chlorophyll is created basically by rather a simple relation with the ambient physical environments.

4.5 Summary and conclusion

We have investigated mechanisms of forming the seasonal variations of the oceanic ecosystem in the North Pacific by using the ecosystem model embedded in the OGCM. The North Pacific can be divided into seven areas on the basis of the seasonal variation patterns of chlorophyll in the model. The factors shaping each pattern are the nutrient concentration which is in turn determined mainly by the vertical velocity, the vertical mixing, and less importantly the light condition. KS and ST in Fig. 4.3 both lie within the downwelling region but can be separated due to the strong vertical mixing in KS from winter to early spring; chlorophyll concentration in KS shows the maximum value in March as the active vertical mixing enriches the surface nutrient. The other areas are all related to the up-

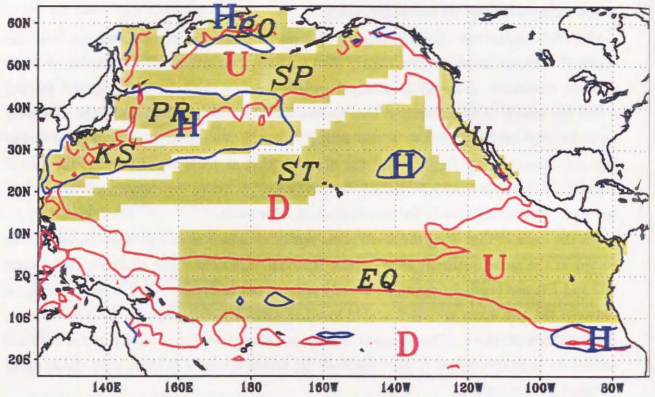

Fig. 4.25. Relation among the areal division, the vertical velocity, and the seasonal variation of mixed layer depth (MLD). The red lines show the contourlines of 0 m/day for the annual mean vertical velocity across the depth of 100 m. The blue lines represent the contourlines of 100 m for the amplitude of the seasonal variation of MLD (difference between the maximum and the minimum MLD). The red letter "U" indicates upwelling, while "D" represents downwelling. The blue letter "H" corresponds to the regions where the MLD amplitude is more than 100 m.

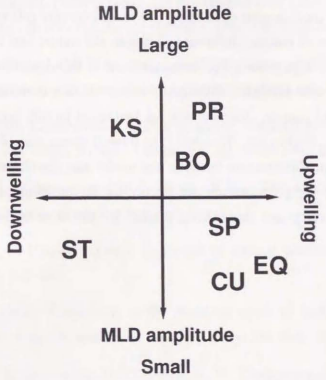

Fig. 4.26. Classification of the areas shown in Fig. 4.3. The vertical axis shows the amplitude of the seasonal variation of mixed layer depth, while the horizontal axis represents the vertical velocity.

welling region, but show different seasonal variations depending on the dynamics of the mixed layer; BO and PR which experience large seasonal variations of the vertical mixing bear blooming when the surface warming leads to the shallow mixed layer; on the other hand, SP, CU, and EQ go through only moderate variations caused by the variation of the light condition and the modest change in the vertical mixing.

The areal division shown in Fig. 4.3 well corresponds to the one by Longhurst (1995) based on observations (Fig. 4.6). Also, the seasonal pattern of each area is reasonably compared with the one observed by satellite measurements and *in situ* observations. Furthermore, most of the mechanisms of forming the variations turn out to have some observational basis. There are, of course, differences between the model and the observations. For example: the modeled high chlorophyll concentration in BO does not last long compared with the CZCS data; the modeled chlorophyll concentration is much lower than that in observations. On these points, chemical and/or biological factors not incorporated in the present model may be important. However, the overall agreement of the seasonal patters of chlorophyll and their distribution between the model and the observations strongly supports the notion that the patterns are set mainly by the ambient physical conditions, of which the vertical velocity and the vertical mixing are the most important.

References

Banse, K. and D. C. English (1994): Seasonality of coastal zone color scanner phytoplankton pigment in the offshore oceans. *J. Geophys. Res.*, **99**, 7323–7345.

Chelton, D. B., P. A. Bernal and J. A. McGowan (1982): Large-scale interannual physical and biological interaction in the California Current. *J. Mar. Res.*, **40**, 1095–1125.

Colebrook, J. M. (1979): Continuous Plankton Records: Seasonal cycles of phytoplankton and copepods in the North Atlantic Ocean and the North Sea. *Mar. Biol.*, **51**, 23–32.

Dugdale, R. C., F. P. Wilkerson and H. J. Minas (1995): The role of a silicate pump in driving new production. *Deep-Sea Res.*, **42**, 697–719.

Evans, G. T. and J. S. Parslow (1985): A model of annual plankton cycles. *Biological Oceanography*, **3**, 327–347.

Fasham, M. J. R. (1995): Variations in the seasonal cycle of biological production in subarctic oceans: A model sensitivity analysis. *Deep-Sea Res.*, **42**, 1111–1149.

Fasham, M. J. R., J. L. Sarmiento, R. D. Slater, H. W. Ducklow and R. Williams (1993): Ecosystem behavior at Bermuda Station S and Ocean Weather Station INDIA: an observational analysis. *Glob. Biogeochem. Cycles*, **7**, 379–415.

Gordon, H. R., D. K. Clark, J. W. Brown and R. H. Evans (1982): Satellite measurements of the phytoplankton pigment concentration in the surface waters of a warm core Gulf Stream ring. *J. Mar. Res.*, **40**, 491–502.

Imai, M., S. Ebara, K. Kawashima, N. Kubo, N. Sato and E. Moriyama (1988): Seasonal variation of chlorophyll-a in the seas around Japan. *Oceanogr. Mag.*, **38**, 23–32.

Levitus, S. and T. P. Boyer (1994): *World Ocean Atlas 1994*, NOAA Atlas NESDIS 4, NODC.

Longhurst, A. (1995): Seasonal cycles of pelagic production and consumption. *Prog. Oceanog.*, **36**, 77–167.

Longhurst, A., S. Sathyendranath, T. Platt and C. Caverhill (1995): An estimate of global primary production in the ocean from satellite radiometer data. *J. Plankton Res.*, **17**, 1245–1271.

Mann, K. H. and J. R. N. Lazier (1991): *Dynamics of Marine Ecosystems*, Blackwell Scientific Publications, Boston, 466pp.

Martin, J. H. and S. E. Fitzwater (1988): Iron deficiency limits phytoplankton growth in the north-east Pacific subarctic. *Nature*, **331**, 341–343.

McCreary, J. P., K. E. Kohler, R. R. Hood and D. B. Olson (1996): A four-compartment ecosystem model of biological activity in the Arabian Sea. *Prog. Oceanog.*, **37**, 193–240.

Obata, A., J. Ishizaka and M. Endoh (1996): Global verification of critical depth theory for phytoplankton bloom with climatological in situ temperature and satellite ocean color data. *J. Geophys. Res.*, **101**, 20,657–20,667.

Parsons, T. R., M. Takahashi and B. Hargrave (1984): *Biological Oceanographic Processes*, Pergamon Press, 3rd edition.

Sambrotto, R. N. and J. J. Goering (1983): Interannual variability of phytoplankton and zooplankton production on the southeast Bering Sea shelf. p. 161–179. In *From year to year*, ed. by W. S. Wooster, A Washington Sea Grant Publication.

Sarmiento, J. L., R. D. Slater, M. J. R. Fasham, H. W. Ducklow, J. R. Toggweiler and G. T. Evans (1993): A seasonal three-dimensional ecosystem model of nitrogen cycling in the North Atlantic euphotic zone. *Glob. Biogeochem. Cycles*, **7**, 417–450.

Smith, S. L. and J. Vidal (1984): Spatial and temporal effects of salinity, temperature and chlorophyll on the communities of zooplankton in the southeastern Bering Sea. *J. Mar. Res.*, **42**, 221–257.

Sverdrup, H. U. (1953): On conditions for the vernal blooming of phytoplankton. *J. Cons. Perm. Int. Exp. Mer.*, **18**, 287–295.

Tabata, S. (1964): *Main Physical Factors Governing the Oceanographic Conditions at Ocean Station "P" in the Norhteast Pacific Ocean*, PhD thesis, Univ. of Tokyo.

Talley, L. D., Y. Nagata, M. Fujimura, T. Iwao, T. Kono, D. Inagake, M. Hirai and K. Okuda (1995): North Pacific intermediate water in the Kuroshio/Oyashio mixed water region. *J. Phys. Oceanogr.*, **25**, 475–501.

Thomas, A. C., F. Huang, P. T. Strub and C. James (1994): Comparison of the seasonal and interannual variability of phytoplankton pigment concentrations in the Peru and California Current system. *J. Geophys. Res.*, **99**, 7355–7370.

Tsunogai, S. and S. Noriki (1983): *Chemical Oceanography — solving the ocean by chemistry*, Sangyo Tosho, in Japanese.

Winn, C. C., R. M. L. C. Campbell, J. R. Christian, D. V. Hebel, J. E. Dore, L. Fujieki and D. M. Karl (1996): Seasonal variability in the phytoplankton community of the North Pacific Subtropical Gyre. *Glob. Biogeochem. Cycles*, **9**, 605–620.

Yoder, J. A., C. R. McClain, G. C. Feldman and W. E. Esaias (1993): Annual cycles of phytoplankton chlorophyll concentrations in the global ocean. *Glob. Biogeochem. Cycles*, **7**, 181–193.

Chapter 5

General Conclusion

Seasonal variation of chlorophyll in the North Pacific has been investigated to clarify the role of physical environments in forming its shape. Understanding of the seasonal variation is definitely needed even for that of the variation of the ecosystem on a longer time scale. For that purpose, the ecosystem model embedded in the OGCM has been developed.

Firstly, the ecosystem model to be incorporated in the OGCM was calibrated with its one-dimensional version. The data used were taken from the two OWSs located in totally different oceanic regimes; one is in the eutrophic and the other in the oligotrophic region. The two sites show distinct contrast that the nutrient is more abundant by the order of magnitude in the former while the chlorophyll concentration and the annual production are of the same order. It turns out that the model reproduces the contrast by changing some of the model parameters between the two sites. The changed parameters are the half saturation constants for nitrate and ammonium, the sinking velocity of PON, and the background vertical diffusion constant. Each of the modifications has a basis from observational or modeling efforts.

Secondly, the ecosystem model was embedded in the OGCM for the North Pacific and the model performance was examined. The parameter values which were changed between the two sites were determined so that the model bears a good result on the basin scale. The OGCM provides fairly good environments for the distribution of MLD and vertical velocity, which are important for the ecosystem modeling. The major defects in the modeled physical environments are the large MLD in March off Sanriku coast and the persistent large MLD on both sides of the equator. The model results for nitrate, chlorophyll, zooplankton, and net primary production were compared with observations on the annual mean basis. The values of the model results are of the same order as in the observations and the overall

feature is that the values of the variables are small in the subtropical region and large in the subpolar and the equatorial region. The model, of course, differs from the observations on some points such as: the chlorophyll concentration which is lower in the subpolar region and higher in the subtropical and the equatorial region than in the CZCS observation; the equatorial NPP which is higher than in the observations; the NPP minimum in the eastern subtropical region where such a minimum can not be found in the observation. On the whole, however, the model shows acceptable performance for an ecosystem model and the results are worth further analysis.

Lastly, the modeled seasonal variation was analyzed. The North Pacific can be divided into seven areas on the basis of the seasonal variation pattern of chlorophyll. The areal division corresponds well to that based on observations. The modeled contrast among the seasonal variation patterns also resembles that in the CZCS observation. The mechanisms forming each of the patterns were examined in detail. It was shown that the key factors determining the seasonal pattern are the nutrient condition and the seasonal variation of the intensity of vertical mixing. The former is, in turn, determined by the annual mean vertical flow. Thus, it is expected that the seasonal patterns can be sorted according to the combination of the annual mean vertical velocity and the amplitude of seasonal variation in MLD. Indeed, the patterns are comprehensively classified based on the two physical factors; areas which have a similar combination of the two to each other do show a similar seasonal variation to each other. Moreover, the spatial extent of each of the patterns is tightly correlated to the distributions of the two physical factors. It is found that the boundaries among the areas coincide well with the selected contourlines of either the vertical velocity or the amplitude of MLD variation. Together with the resemblance between the model results and the observation, the analysis suggests the dominance of the two physical factors over chemical and/or biological factors in shaping the seasonal variation.

One of the problems the model is applied to in the future is the ecosystem variation on the decadal time scale. Many observational studies on this subject suggest that the MLD variation associated with the climate variation on this time scale is responsible for the ecosystem variation. Thus, it is important for an ecosystem model to be able to reproduce regional differences on how the ecosystem reacts to changes in MLD. The model results did show the model's ability to reproduce them on the seasonal time scale. As stated in Chapter 1, ability in reproduction of the seasonal variation is the basis for the prediction of the variation on the decadal time scale; for example, the biological activities in the

oligotrophic region are enhanced when the mixed layer deepens and the reverse is true in the eutrophic region as discussed in Chapter 2; this realistic feature will remain on the decadal time scale as it should be for studying the decadal ecosystem variation. Thus, the results obtained in this thesis are encouraging for the future application to this issue.

There are, however, some problems in the model that need to be solved. The increasing trend of the nitrate concentration should be eliminated by seeking a better set of parameter values. The density structure in the surface layer in the OGCM also showed disagreements with observation such as: the halocline in the subpolar region that is too shallow; the mixed layer beside the equator that is too deep; the mixed layer off Sanriku coast that is too deep in March. Some of the defects in the OGCM will be overcome in a finer horizontal resolution model.